out of 10). Following the treatment with 0.1 μg/ml of MPTP, the skin became darkly pigmented as in the MPTP-treated zebrafish (Fig. 3A and B), presumably due to the impairment of peripheral catecholaminergic nerves (Bretaud et al., 2004). However there was no significant decrease in the number of TH^+ cells in the diencephalon and medulla oblongata, nor in the level of spontaneous swimming movement of the MPTP-treated adult medaka at 0.1 μg/ml (data not shown). Prolonged exposure of up to 3 weeks also did not alter the number of TH^+ neurons nor the spontaneous movement (Fig. 3C, data not shown).

Next, we sought to determine the effect of MPTP on medaka larvae since higher sensitivity of TH^+ neurons to MPTP has been reported in zebrafish larvae compared to the adult (McKinley et al., 2005). When medaka larvae were treated with 0.2 μg/ml of MPTP for 2 days, 35 out of 50 (70%) fish survived, while only 1 out 10 (10%) survived after the treatment with 0.3 μg/ml of MPTP. The cytotoxic effect of MPTP on dopaminergic neurons in larvae was then determined by the whole mount immunohistochemistry 3 days after the end of exposure to 0.2 μg/ml of MPTP. In contrast to the fish exposed to MPTP at the adult stage, the TH^+ signal in the diencephalon was markedly decreased in the fish exposed to MPTP at the larval stage (Fig. 4C). The quantitative analysis showed 84% decrease in the TH^+ signal in the MPTP-treated fish compared to the non-treated control (Fig. 4E). These results indicate that the MPTP elicits the reduction of TH^+ neurons in medaka larvae, but not in the adult fish.

Since the histological analysis showed that MPTP impaired dopaminergic neurons, we monitored the spontaneous swimming movement of larvae exposed to 0.2 μg/ml of MPTP using the automated tracking system. Starting immediately after the end of exposure, MPTP-treated fish showed marked decrease in the total swimming distance (Fig. 5A). Additionally, the MPTP treatment significantly diminished the frequency and velocity of swimming (Fig. 5B and C). Although 0.2 μg/ml of MPTP is much lower than the concentration used in previous reports in zebrafish (5–45 μg/ml) (McKinley et al., 2005; Wen et al., 2008; Bretaud et al., 2004), even lower concentration of MPTP (0.02 μg/ml) showed the reduction in both the number of TH^+ neurons and the spontaneous movement (Fig. 5A–D). The group treated with 0.02 μg/ml of MPTP exhibited the intermediate phenotype between the control and the group treated with 0.2 μg/ml of MPTP, suggesting the dose–response relationship. To exclude the possibility of symptoms other than PD, we forced the fish to swim by giving them a touch or sound stimulus. We found that MPTP-treated fish and their untreated controls displayed comparable quick response to these stimuli (data not shown), suggesting that MPTP affects the spontaneous movement of medaka without associating with muscle weakness, paralysis and sensory defect.

3.3. Persistent loss of dopaminergic neurons in the brain of medaka exposed to MPTP at the larval stage

Not a few studies have revealed the cytotoxic effect of MPTP on TH^+ cells in teleost fish (Pollard et al., 1992; Anichtchik et al., 2004; Wen et al., 2008; Bretaud et al., 2004; Lam et al., 2005; McKinley

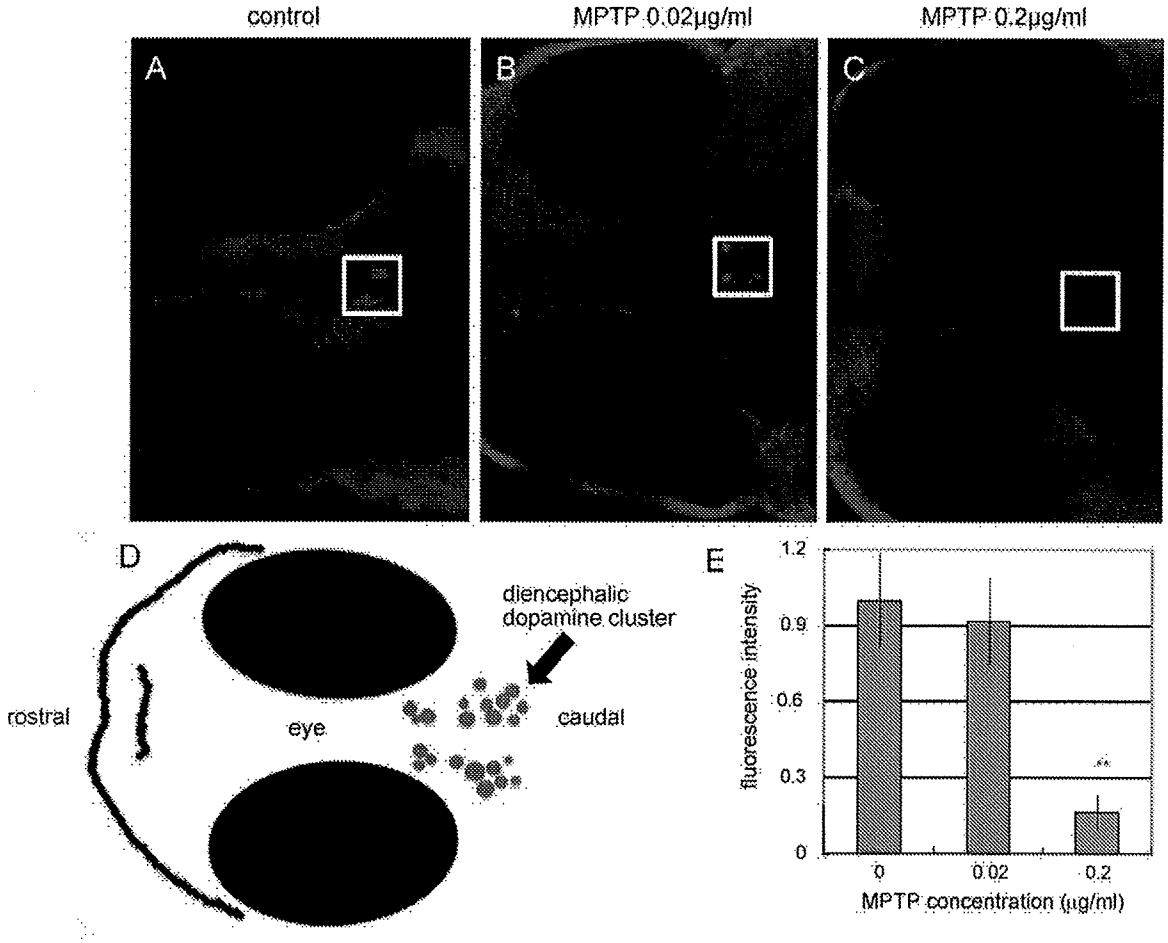

Fig. 4. Whole mount TH staining of medaka larvae following exposure to MPTP. White squares indicated diencephalic dopamine neurons. Images were taken 5 days after the first exposure (15-dpf) (A: control, B: MPTP 0.02 μg/ml and C: MPTP 0.2 μg/ml), and were used quantitative analysis. (D) Showed simple atlas of the images. (E) Quantitative comparisons of the fluorescence of TH^+ neurons. The region of interest was set as a minimal square including TH^+ neurons in the diencephalon. 0.2 μg/ml MPTP treatment markedly reduced TH^+ signals in the diencephalon (C and E). $^{**}p < 0.01$ vs. control. $n = 4$ for each group.

et al., 2005). However, it is important to investigate the long-term effect of MPTP-induced depletion of dopaminergic neurons because it has been known that the fish has a strong regenerative capacity of the brain structures (Zupanc, 2008). To this end, we exposed 10-dpf larvae to 0.2 μg/ml MPTP for 2 days, and measured the amounts of both dopamine and 3,4-dihydroxyphenylacetic acid (DOPAC), a metabolite of dopamine, in the whole brain at 3 months after the MPTP treatment. We verified that both dopamine and DOPAC of the whole brain significantly decreased in MPTP-treated fish in comparison with non-treated control fish (Fig. 6A and B). DOPAC/dopamine ration was increased significantly and this was consistent with other MPTP models (Fig. 6D) (Irwin et al., 1990). The reduction of dopamine and DOPAC may not reflect general toxicity of MPTP towards the whole neurons, because MPTP did not diminish the level of norepinephrine (Fig. 6C).

To confirm whether MPTP injured the cluster of the diencephalic TH^+ neurons, leading to the decline of dopamine content in the brain, we counted the number of TH^+ cells in the brain. The number of TH^+ dopaminergic neurons in the middle diencephalon was significantly less in the MPTP-treated group than that in the non-treated control group (Fig. 7A–C). In contrast to the dopaminergic neurons in the middle diencephalon, the TH^+ signal intensity of dopaminergic fibers in the telencephalon were scarcely affected by MPTP possibly reflecting the recovery of these fibers after MPTP exposure at their larval stage (data not shown). The number of TH^+ neurons in the rostro-ventral and the caudal part of the diencephalon, and in the medulla oblongata also did not show statistically significant differences (Fig. 7C). Western blot analysis of whole brain extract disclosed a slight, albeit not statistically significant, decrease in the level of TH protein in the MPTP-treated groups (Fig. 7D). These data suggest that MPTP imposed on the

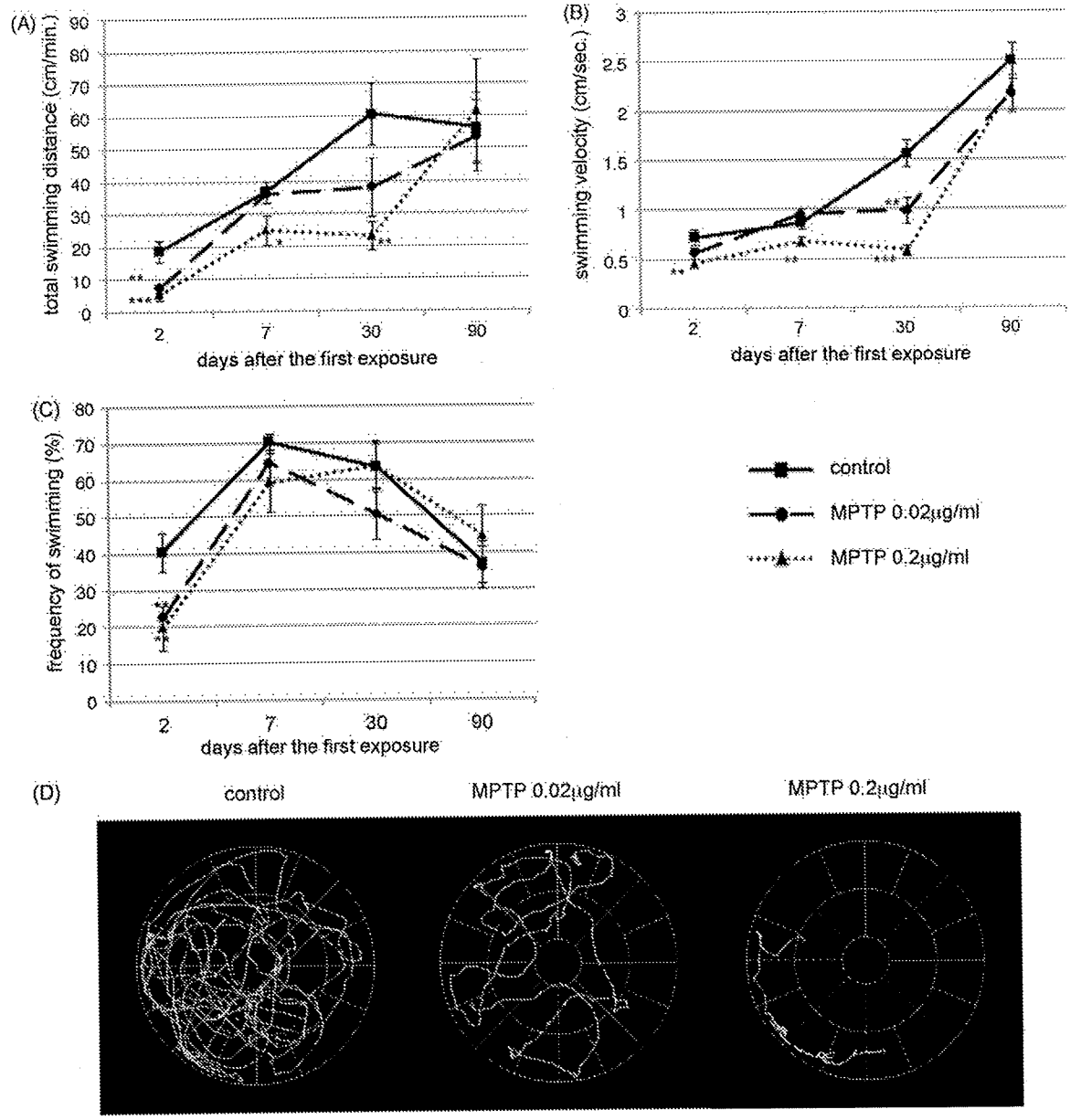

Fig. 5. Spontaneous movement analysis of MPTP-treated medaka. (A) Total swimming distance (cm/min), (B) swimming velocity (cm/s), (C) frequency of swimming movement (%), (D) representative swimming track immediately after the 2 days exposure of MPTP. Total swimming distance and swimming velocity of 0.2 μg/ml MPTP-treated fish decreased significantly 2, 7 and 30 days after the first exposure (12, 17 and 40-dpf) (A, B and D). The frequency of swimming movement also decreased 2 days after the first exposure (12-dpf) (C). The MPTP-treated fish showed gradual recovery from the defective movement and all the parameters did not differ among the groups 90 days after the first exposure (100-dpf) (A–C). $^*p < 0.05$, $^{**}p < 0.01$, $^{***}p < 0.001$ vs. control. $n = 10$ for each group.

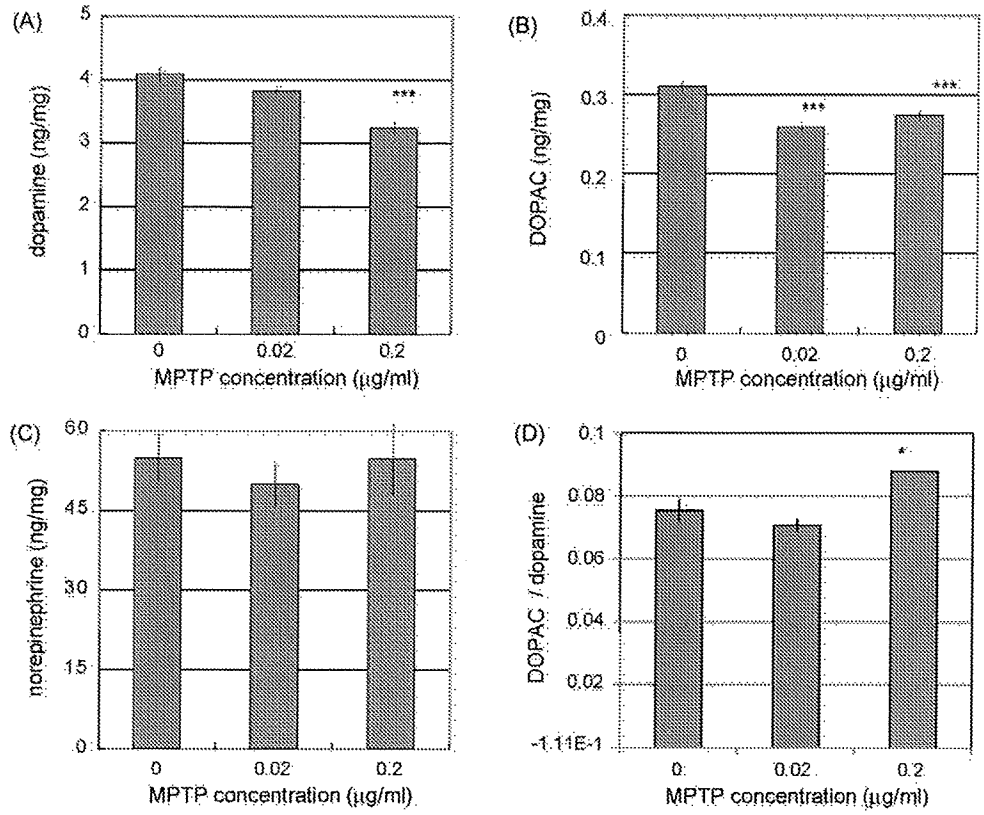

Fig. 6. HPLC analysis of neuro-transmitters in MPTP-treated medaka. Dopamine (A), DOPAC (B) and norepinephrine (C) amount in the whole brain of adult (100-dpf) medaka treated with water (control), 0.02 μg/ml MPTP and 0.2 μg/ml MPTP at the larval stage. All values are presented as the amount (ng) per protein weight (mg). Dopamine and DOPAC were decreased in 0.2 μg/ml MPTP-treated fish (A and B). Norepinephrine did not differ among the groups (C). (D) Showed DOPAC/dopamine ratio. $^{*}p < 0.05$, $^{***}p < 0.001$ vs. control. $n = 8$ for each group.

larval stage causes selective and persistent loss of the middle diencephalic TH^+ neurons after 3 months of exposure.

Next, we investigated a long-term effect of MPTP on neurological function by monitoring the spontaneous swimming movement of medaka over time. One month after the exposure, the frequency of swimming movement in MPTP-treated group completely recovered to the level of non-treated fish (Fig. 5C), although the total swimming distance and the velocity of swimming still decreased in MPTP-treated group (Fig. 5A and B). Three months after the exposure, the MPTP-treated group displayed the complete recovery of all the parameters of swimming movement tested (Fig. 5A–C). In summary, although MPTP treatment at the larval stage may irreversibly damage specific cluster of diencephalic TH^+ neurons and thereby decrease the amount of dopamine in the whole brain, the suppressive effect of MPTP on the spontaneous movement is observed only transiently and disappears 3 months after the exposure to MPTP.

4. Discussion

We here identified TH^+ dopaminergic neurons and noradrenergic neurons in the medaka brain. The larvae exposed to MPTP showed dopaminergic cell loss and reduced spontaneous movement. When these fish reached to an adult stage, they still displayed the loss of dopaminergic neurons associated with reduced amounts of dopamine in the whole brain, although the movement deficit gradually recovered to the normal level. Remarkably, MPTP-induced neuronal loss was restricted to the middle diencephalic clusters, which may include substantia nigra-like structure in teleosts. Therefore, we reasoned that the MPTP treatment at the larval stage allows the establishment of a medaka model of PD.

We demonstrated the specific toxicity of MPTP towards TH^+ neurons in the middle diencephalon. Other TH^+ neurons including diencephalic neurons outside this region and the neurons in medulla oblongata did not show the reduction in number. The vulnerability of the neurons in the paraventricular area of the middle diencephalon to MPTP, together with their anatomical features, supports the idea that these cells are the bona fide an equivalent of the substantia nigra in mammals. Toxic effect of MPTP specific to diencephalic TH^+ neurons was also reported in zebrafish (McKinley et al., 2005; Wen et al., 2008; Bretaud et al., 2004). By contrast, several other reports showed the reduction of not only dopaminergic but also norepinephrinergic neurons in MPTP-treated zebrafish and goldfish (Pollard et al., 1992; Anichtchik et al., 2004). The differential toxic effects of MPTP on norepinephrinergic neurons may depend on the routes of drug administration, as we noticed that in these reports the injection of MPTP into adult fish led to the injury of norepinephrinergic neurons, whereas submerging the fish in the water containing MPTP affected only dopaminergic neurons. We speculate that the pharmacodynamics is quite different between these two methods, with injection leading to a very high concentration in various tissues. Recent report showed the broad toxicity of MPTP not only on dopaminergic neurons but also on noradrenergic and histaminergic neurons even though they exposed zebrafish to the water containing MPTP (Sallinen et al., 2009). Because the amount of MPTP they used is much higher than our report, we speculate that this may be due to the broader spectrum injury of MPTP.

It is also an intriguing question whether the peripheral tissue is damaged by MPP^+ generated by peripheral MAO-B as suggested by MPTP-induced skin color change (Fig. 3A and B). The metabolic pathway and distribution of MPTP and MPP^+ in medaka should be investigated in the future.

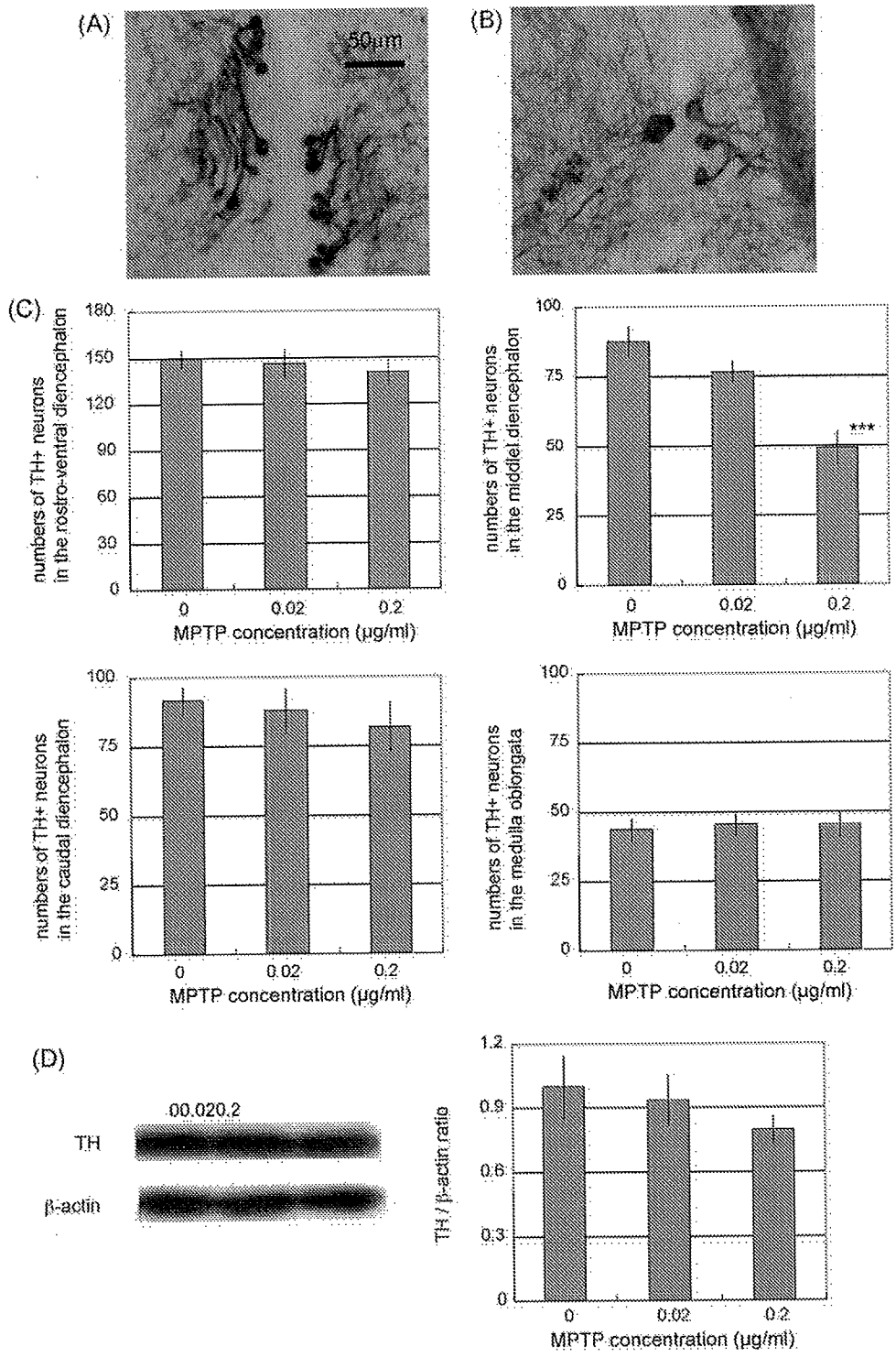

Fig. 7. TH immunohistochemistry and western blotting of adult medaka treated with MPTP at their larval stage. Samples were fixed 90 days after the first exposure (100-dpf). Coronal sections taken from the diencephalon level showed TH^+ neurons in control fish (A) and 0.2 μg/ml MPTP-treated fish (B). The numbers of TH^+ neurons in the middle diencephalon decreased significantly in MPTP-treated medaka (C). The numbers of TH^+ neurons in the rostro-ventral and caudal diencephalon, and the medulla oblongata did not show significant differences (C). $^{***}p < 0.001$ vs. control. $n = 8$ for each group. (D) The protein amount of TH in the whole brain of the control, 0.02 μg/ml MPTP-treated and 0.2 μg/ml MPTP-treated fish is examined by western blotting and then normalized by β-actin (loading control). The graph shows the ratio of TH/β-actin amount in each genotype (the average amount of control fish = 1). The amount of TH protein did not differ significantly among the groups. $n = 4$ for each group.

Previous studies of zebrafish and goldfish did not follow the long time course of MPTP toxicity, but continuous observation is important for the model animal because of the following reasons. First, PD is a late-onset and long-lasting neurodegenerative disorder. Second, the brains of teleost fish show widespread adult neurogenesis and new TH^+ cells are added in the olfactory bulb and diencephalon (Grandel et al., 2006). We here show the gradual functional recovery of dopaminergic neurons in the fish transiently exposed to MPTP at the larval stage, as evidenced by increases in spontaneous movement. Such behavioral recovery has been reported in several mammalian species after MPTP treatment (Rose et al., 1989; Elsworth et al., 1990, 2000; Kurlan et al., 1991).

The degree of the recovery is variable and may be dependent on several factors, including the protocol of MPTP treatment, the species, and the method of behavioral evaluation. Interestingly, the functional recovery observed in medaka was not accompanied by the restoration of the number of TH^+ cells or by increase in the amount of dopamine to a normal level in the adult stage. The striatum of MPTP-treated medaka did not show robust denervation of the TH^+ neurons, and this may explain the behavioral recovery observed in our medaka. Such complete behavioral recovery despite the incomplete return of the amount of dopamine may take place as in squirrel monkeys, possibly due to alteration in dopamine metabolism and neuronal sprouting (Petzinger et al., 2006).

In summary we have generated a medaka PD model by treating larval fish with MPTP, and established reliable assays from the larval stage to the adult. Our protocol of inducing PD-like phenotypes and our assay described in this study provides invaluable tools to investigate medaka model of familial PD retrieved from the TILLING library or medaka treated by other toxins or drugs.

Acknowledgements

We are grateful to all the technical staff of the Department of Radiation Genetics and all the people of the Department of Neurology.

Appendix A. Supplementary data

Supplementary data associated with this article can be found, in the online version, at doi:10.1016/j.neures.2009.07.010.

References

Aida, T., 1921. On the inheritance of color in a fresh-water fish, *Aplocheilus latipes* Temminck and Schlegel, with special reference to sex-linked inheritance. Genetics 6, 554–573.

Anichtchik, O.V., Kaslin, J., Peitsaro, N., Scheinin, M., Panula, P., 2004. Neurochemical and behavioral changes in zebrafish *Danio rerio* after systemic administration of 6-hydroxydopamine and 1-methyl-4-phenyl-1,2,3,6-tetrahydropyridine. J. Neurochem. 88, 443–453.

Bonifati, V., Rizzu, P., van Baren, M.J., Schaap, O., Breedveld, G.J., Krieger, E., Dekker, M.C., Squitieri, F., Ibanez, P., Joosse, M., van Dongen, J.W., Vanacore, N., van Swieten, J.C., Brice, A., Meco, G., van Duijn, C.M., Oostra, B.A., Heutink, P., 2003. Mutations in the DJ-1 gene associated with autosomal recessive early-onset parkinsonism. Science 299, 256–259.

Bové, J., Prou, D., Perier, C., Przedborski, S., 2005. Toxin-induced models of Parkinson's disease. NeuroRx 2, 484–494.

Bretaud, S., Lee, S., Guo, S., 2004. Sensitivity of zebrafish to environmental toxins implicated in Parkinson's disease. Neurotoxicol. Teratol. 26, 857–864.

Cauchi, R.J., van den Heuvel, M., 2006. The fly as a model for neurodegenerative diseases: is it worth the jump? Neurodegener. Dis. 3, 338–356.

Elsworth, J.D., Deutch, A.Y., Redmond Jr., D.E., Sladek Jr., J.R., Roth, R.H., 1990. MPTP-induced parkinsonism: relative changes in dopamine concentration in subregions of substantia nigra, ventral tegmental area and retrorubral field of symptomatic and asymptomatic vervet monkeys. Brain Res. 513, 320–324.

Elsworth, J.D., Taylor, J.R., Sladek Jr., J.R., Collier, T.J., Redmond Jr., D.E., Roth, R.H., 2000. Striatal dopaminergic correlates of stable parkinsonism and degree of recovery in old-world primates one year after MPTP treatment. Neuroscience 95, 399–408.

Fleming, S.M., Fernagut, P.O., Chesselet, M.F., 2005. Genetic mouse models of parkinsonism: strengths and limitations. NeuroRx 2, 495–503.

Gasser, T., 2005. Genetics of Parkinson's disease. Curr. Opin. Neurol. 18, 363–369.

Gerlach, M., Riederer, P., Przuntek, H., Youdim, M.B., 1991. MPTP mechanisms of neurotoxicity and their implications for Parkinson's disease. Eur. J. Pharmacol. 208, 273–286.

Grandel, H., Kaslin, J., Ganz, J., Wenzel, I., Brand, M., 2006. Neural stem cells and neurogenesis in the adult zebrafish brain: origin, proliferation dynamics, migration and cell fate. Dev. Biol. 295, 263–277.

Irwin, I., DeLanney, L.E., Forno, L.S., Finnegan, K.T., Di Monte, D.A., Langston, J.W., 1990. The evolution of nigrostriatal neurochemical changes in the MPTP-treated squirrel monkey. Brain Res. 531, 242–252.

Kapsimali, M., Bourrat, F., Vernier, P., 2001. Distribution of the orphan nuclear receptor Nurr1 in medaka (*Oryzias latipes*): cues to the definition of homologous cell groups in the vertebrate brain. J. Comp. Neurol. 431, 276–292.

Kasahara, M., Naruse, K., Sasaki, S., Nakatani, Y., Qu, W., Ahsan, B., Yamada, T., Nagayasu, Y., Doi, K., Kasai, Y., Jindo, T., Kobayashi, D., Shimada, A., Toyoda, A., Kuroki, Y., Fujiyama, A., Sasaki, T., Shimizu, A., Asakawa, S., Shimizu, N., Hashimoto, S., Yang, J., Lee, Y., Matsushima, K., Sugano, S., Sakaizumi, M., Narita, T., Ohishi, K., Haga, S., Ohta, F., Nomoto, H., Nogata, K., Morishita, T., Endo, T., Shin-I, T., Takeda, H., Morishita, S., Kohara, Y., 2007. The medaka draft genome and insights into vertebrate genome evolution. Nature 447, 714–719.

Kitada, T., Asakawa, S., Hattori, N., Matsumine, H., Yamamura, Y., Minoshima, S., Yokochi, M., Mizuno, Y., Shimizu, N., 1998. Mutations in the parkin gene cause autosomal recessive juvenile parkinsonism. Nature 392, 605–608.

Kurlan, R., Kim, M.H., Gash, D., 1991. The time course and magnitude of spontaneous recovery of parkinsonism produced by intracarotid administration of 1-methyl-4-phenyl-1,2,3,6-tetrahydropyridine to monkeys. Ann. Neurol. 29, 677–679.

Lam, C.S., Korzh, V., Strahle, U., 2005. Zebrafish embryos are susceptible to the dopaminergic neurotoxin MPTP. Eur. J. Neurosci. 21, 1758–1762.

McKinley, E.T., Baranowski, T.C., Blavo, D.O., Cato, C., Doan, T.N., Rubinstein, A.L., 2005. Neuroprotection of MPTP-induced toxicity in zebrafish dopaminergic neurons. Brain Res. Mol. Brain Res. 141, 128–137.

Outeiro, T.F., Lindquist, S., 2003. Yeast cells provide insight into alpha-synuclein biology and pathobiology. Science 302, 1772–1775.

Paisán-Ruíz, C., Jain, S., Evans, E.W., Gilks, W.P., Simón, J., van der Brug, M., López de Munain, A., Aparicio, S., Gil, A.M., Khan, N., Johnson, J., Martinez, J.R., Nicholl, D., Carrera, I.M., Pena, A.S., de Silva, R., Lees, A., Martí-Massó, J.F., Pérez-Tur, J., Wood, N.W., Singleton, A.B., 2004. Cloning of the gene containing mutations that cause PARK8-linked Parkinson's disease. Neuron 44, 595–600.

Petzinger, G.M., Fisher, B., Hogg, E., Abernathy, A., Arevalo, P., Nixon, K., Jakowec, M.W., 2006. Behavioral motor recovery in the 1-methyl-4-phenyl-1,2,3,6-tetrahydropyridine-lesioned squirrel monkey (*Saimiri sciureus*): changes in striatal dopamine and expression of tyrosine hydroxylase and dopamine transporter proteins. J. Neurosci. Res. 83, 332–347.

Pollard, H.B., Dhariwal, K., Adeyemo, O.M., Markey, C.J., Caohuy, H., Levine, M., Markey, S., Youdim, M.B., 1992. A parkinsonian syndrome induced in the goldfish by the neurotoxin MPTP. FASEB J. 6, 3108–3116.

Polymeropoulos, M.H., Lavedan, C., Leroy, E., Ide, S.E., Dehejia, A., Dutra, A., Pike, B., Root, H., Rubenstein, J., Boyer, R., Stenroos, E.S., Chandrasekharappa, S., Athanassiadou, A., Papapetropoulos, T., Johnson, W.G., Lazzarini, A.M., Duvoisin, R.C., Di Iorio, G., Golbe, L.I., Nussbaum, R.L., 1997. Mutation in the alpha-synuclein gene identified in families with Parkinson's disease. Science 276, 2045–2047.

Rink, E., Wullimann, M.F., 2004. Connections of the ventral telencephalon (subpallium) in the zebrafish (*Danio rerio*). Brain Res. 1011, 206–220.

Rogaeva, E., Johnson, J., Lang, A.E., Gulick, C., Gwinn-Hardy, K., Kawarai, T., Sato, C., Morgan, A., Werner, J., Nussbaum, R., Petit, A., Okun, M.S., McInerney, A., Mandel, R., Groen, J.L., Fernandez, H.H., Postuma, R., Foote, K.D., Salehi-Rad, S., Liang, Y., Reimsnider, S., Tandon, A., Hardy, J., St George-Hyslop, P., Singleton, A.B., 2004. Analysis of the PINK1 gene in a large cohort of cases with Parkinson disease. Arch. Neurol. 61, 1898–1904.

Rose, S., Nomoto, M., Jenner, P., Marsden, C.D., 1989. Transient depletion of nucleus accumbens dopamine content may contribute to initial akinesia induced by MPTP in common marmosets. Biochem. Pharmacol. 38, 3677–3681.

Sallinen, V., Torkko, V., Sundvik, M., Reenilä, I., Khrustalyov, D., Kaslin, J., Panula, P., 2009. MPTP and MPP+ target specific aminergic cell populations in larval zebrafish. J. Neurochem. 108, 719–731.

Shimamura, K., Takeichi, M., 1992. Local and transient expression of E-cadherin involved in mouse embryonic brain morphogenesis. Development 116, 1011–1019.

Taniguchi, Y., Takeda, S., Furutani-Seiki, M., Kamei, Y., Todo, T., Sasado, T., Deguchi, T., Kondoh, H., Mudde, J., Yamazoe, M., Hidaka, M., Mitani, H., Toyoda, A., Sakaki, Y., Plasterk, R.H., Cuppen, E., 2006. Generation of medaka gene knockout models by target-selected mutagenesis. Genome Biol. 7, R116.

Valente, E.M., Abou-Sleiman, P.M., Caputo, V., Muqit, M.M., Harvey, K., Gispert, S., Ali, Z., Del Turco, D., Bentivoglio, A.R., Healy, D.G., Albanese, A., Nussbaum, R., González-Maldonado, R., Deller, T., Salvi, S., Cortelli, P., Gilks, W.P., Latchman, D.S., Harvey, R.J., Dallapiccola, B., Auburger, G., Wood, N.W., 2004. Hereditary early-onset Parkinson's disease caused by mutations in PINK1. Science 304, 1158–1160.

van Ham, T.J., Thijssen, K.L., Breitling, R., Hofstra, R.M., Plasterk, R.H., Nollen, E.A., 2008. *C. elegans* model identifies genetic modifiers of alpha-synuclein inclusion formation during aging. PLoS Genet. 4, e1000027.

Wen, L., Wei, W., Gu, W., Huang, P., Ren, X., Zhang, Z., Zhu, Z., Lin, S., Zhang, B., 2008. Visualization of monoaminergic neurons and neurotoxicity of MPTP in live transgenic zebrafish. Dev. Biol. 314, 84–92.

Wittbrodt, J., Shima, A., Schartl, M., 2002. Medaka—a model organism from the far east. Nat. Rev. Genet. 3, 53–64.

Yang, H., Tiersch, T.R., 2009. Current status of sperm cryopreservation in biomedical research fish models: zebrafish, medaka, and Xiphophorus. Comp. Biochem. Physiol. C: Toxicol. Pharmacol. 149, 224–232.

Zimprich, A., Biskup, S., Leitner, P., Lichtner, P., Farrer, M., Lincoln, S., Kachergus, J., Hulihan, M., Uitti, R.J., Calne, D.B., Stoessl, A.J., Pfeiffer, R.F., Patenge, N., Carbajal, I.C., Vieregge, P., Asmus, F., Müller-Myhsok, B., Dickson, D.W., Meitinger, T., Strom, T.M., Wszolek, Z.K., Gasser, T., 2004. Mutations in LRRK2 cause autosomal-dominant parkinsonism with pleomorphic pathology. Neuron 44, 601–607.

Zupanc, G.K., 2008. Adult neurogenesis and neuronal regeneration in the brain of teleost fish. J. Physiol. Paris 102, 357–373.

Epilepsia, **(*):1–4, 2009
doi: 10.1111/j.1528-1167.2009.02309.x

BRIEF COMMUNICATION

Mutations in *LGI1* gene in Japanese families with autosomal dominant lateral temporal lobe epilepsy: The first report from Asian families

*Jun Kawamata, *Akio Ikeda, *Youshi Fujita, †[1]Keiko Usui, *[2]Shun Shimohama, and *Ryosuke Takahashi

*Department of Neurology and †Human Brain Research Center, Kyoto University Graduate School of Medicine, Shogoin, Sakyo-ku, Kyoto, Japan

Summary

Autosomal dominant lateral temporal lobe epilepsy (ADLTE) caused by *LGI1* (leucine-rich gene, glioma-inactivated-1) mutations is a rare familial epileptic syndrome characterized by the auditory ictal manifestation and rare nocturnal generalized seizures. We have examined the sequence of the *LGI1* gene in four Japanese families with lateral temporal lobe epilepsy having characteristic auditory features, and identified one novel (1421G>A), and one reported (1418C>T) point mutation each in two families. These two mutations were 3 bp apart in the *LGI1* gene and caused adjoining amino acid substitutions. The two families presented different clinical phenotypes and seizure control to drug treatment. These findings suggest that *LGI1* mutations in Japanese ADLTE families may not be uncommon, and that diverse clinical phenotypes make adequate diagnosis of ADLTE difficult when only based on clinical information.

KEY WORDS: ADLTE, *LGI1*, Mutation, Psychiatric symptoms, Panic attack–like symptoms.

Autosomal dominant lateral temporal lobe epilepsy (ADLTE, MIM 600512) is a rare form of lateral temporal lobe epilepsy with characteristic manifestations such as auditory and visual auras, seizures triggered by auditory stimuli, and rare nocturnal generalized seizures (Gu et al., 2005). The majority of hereditary idiopathic epileptic disorders are caused by mutations of genes encoding ion channel components. The only exception in human so far is ADLTE, which is caused by mutations in *LGI1*, leucine-rich glioma inactivated-1, a gene encoding a secreted neuronal protein (Fukata et al., 2006).

In 1995, the linkage analysis of a large family with partial epilepsy showed strong evidence for localization of a gene for partial epilepsy on 10q22-24 (Ottman et al., 1995). In 2002 the *LGI1* was identified as a causative gene, and its mutations in five families with ADLTE were reported (Kalachikov et al., 2002). To date more than 13 point mutations with amino acid substitutions and one insertion, five deletions, three point mutations resulting in premature truncations, and one point mutation resulting in skipping two exons have been reported (Morante-Redolat et al., 2002; Fertig et al., 2003; Gu et al., 2005; Chabrol et al., 2007). No pathologic polymorphism was found in the promoter region of *LGI1* (Bovo et al., 2008). Clinical semiology seems to vary among families, but no analyses with regard to the different ethnics were done because of absence of reports of ADLTE from Asian countries. Herein we report the first, non-Caucasian ADLTE families with *LGI1* mutations. The content of this article has not appeared elsewhere except for in abstract form (Ikeda et al., 2007).

Accepted July 24, 2009; Early View publication Xxxx xx, 2009.

Address correspondence to Akio Ikeda, M.D., Ph.D., Department of Neurology, Kyoto University Graduate School of Medicine, 54 Shogoin-Kawaharacho, Sakyo-ku, Kyoto 606-8507, Japan. E-mail: akio@kuhp.kyoto-u.ac.jp

Present addresses: [1]National Epilepsy Center, Shizuoka Institute of Epilepsy and Neurological Disorders, Shizuoka, Japan.

[2]Department of Neurology, Sapporo Medical University School of Medicine, Sapporo, Hokkaido, Japan.

Subjects and Methods

Subjects

In 2005 and 2006, we had four families who were clinically consistent with a diagnosis of ADLTE. They were treated for their seizure disorders at Kyoto University Hospital and resided in Kyoto province. Two families of four carried different heterozygous mutations in the *LGI1* gene,

the family "O" and the family "U" (Figs. 1 and 2). Two patients in the family "O" and three patients in the family "U" were treated for their seizure disorders and psychiatric symptoms at Kyoto University Hospital. The detailed clinical manifestation of the two families is described in the Results.

Gene analysis

Genetic analysis of ADLTE was approved by the Kyoto University Graduate School of Medicine Ethical Committee, and written informed consent was obtained from all the patients and the control participants investigated in the present study. DNA from the five patients in the four families were analyzed in this study. The control sample consisted of DNA from 50 healthy Japanese volunteers who gave informed consent. Using primers previously reported, eight exons of the *LGI1* gene were amplified and subsequently sequenced on an ABI310 sequencer (Applied Biosystems, Foster City, CA, U.S.A.) (Michelucci et al., 2003). Mutations in the *LGI1* gene were confirmed by NruI restriction enzyme digestion.

Results

Clinical manifestation

Family "O" had a history of epilepsy in nine members in five generations (Fig. 1). A proband, IV-5, a 27-year-old-woman, had the first generalized tonic–clonic seizure (GTCS) at the age of 10 years while asleep. Currently she has GTCSs every 1–2 months, almost daily auras, and weekly complex partial seizure (CPS), despite high-dose polytherapy such as carbamazepine, zonisamide, and clonazepam. The patient had several types of auras as follows. Auditory auras consisted of high-pitched sound, becoming gradually louder, resulting in inability to understand the spoken language (aphasic state). Visual auras were elementary, flashing light, and metamorphopsia. The patient also had déjà vu, jamais vu, and autonomic auras (i.e., palpitation, cold sweat, and pale face). All of the auras occurred in various combinations and also occurred independently. Those auras, especially the latter ones, were frequently followed by panic attack–like symptoms (i.e., sudden onset of fear and anxiety). The patient also confessed that she had auditory hallucination that she should throw her child out of the window. This occurred independent of the ordinary auras described above. Electroencephalography (EEG) showed no clear epileptiform discharges, despite repetitive sleep EEGs, and magnetic resonance imaging (MRI) showed the small volume of the left superior temporal gyrus. Fluorodeoxyglucose–positron emission tomography (FDG-PET) by statistical parametric mapping (SPM) analysis revealed decreased glucose metabolism in the left lateral temporal area.

The younger sister of the proband, IV-7, a 26-year-old-woman, also had the first GTCS while asleep at the age of 11 years, and currently has GTCSs once a year, and auditory auras (high-pitched sound) and déjà vu, each several times per week. The patient had no visual auras, jamais vu, autonomic auras, or psychiatric symptoms such as anxiety attacks. It was reported that EEG showed no clear epileptiform discharges.

Among their family members, four had apparent psychiatric symptoms such as an outrage of emotion and extraordinary explosive violent behaviors. One of them (II-12) was admitted to the psychiatric hospital for several months, and two of them (II-9 and II-12) had sudden death. Five had both psychiatric symptoms and seizures like the proband. For seizure disorders, at least five (II-12, III-2, III-3, IV-5, and IV-7)

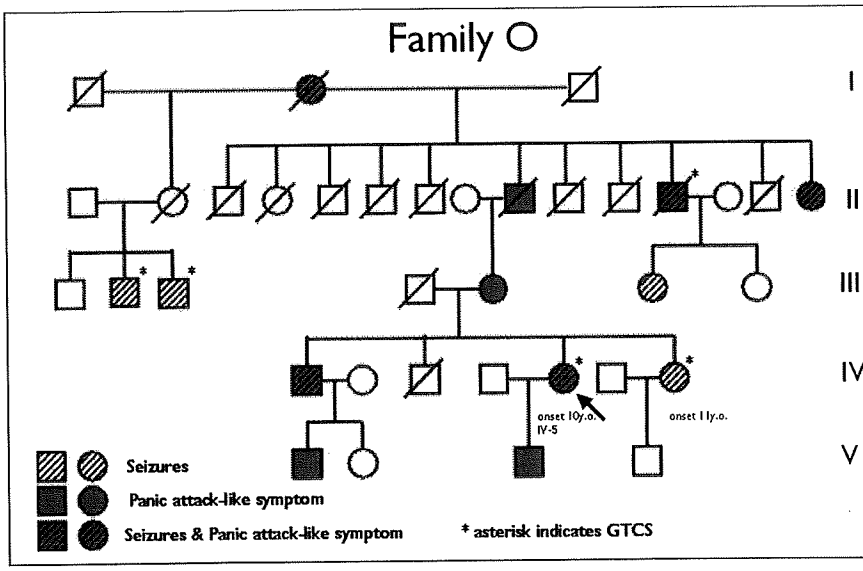

Figure 1.
Pedigree of a five-generation family "O" with autosomal dominant lateral temporal lobe epilepsy (ADLTE). The proband case is indicated by the arrow. The DNA samples from IV-5 and IV-7 carry 1418C>T mutation in the *LGI1* gene. The clinical significance of this family is the diversity of the symptoms, for example, panic attack–like symptoms and seizures with auditory features. It seems that the affected phenotype of seizure skips generations.
Epilepsia © ILAE

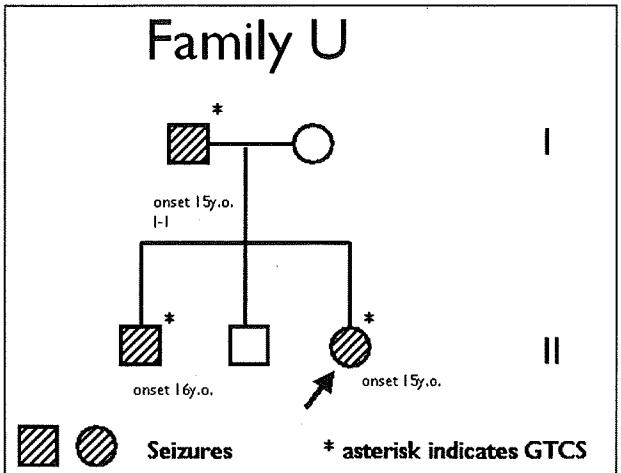

Figure 2.
Pedigree of a two-generation family "U" with autosomal dominant lateral temporal lobe epilepsy (ADLTE). The proband case is indicated by the arrow. The DNA sample from I-1 (the father of the proband) carries 1421G>A mutation in the *LGI1* gene (cited from Ikeda et al., 2000, with permission).
Epilepsia © ILAE

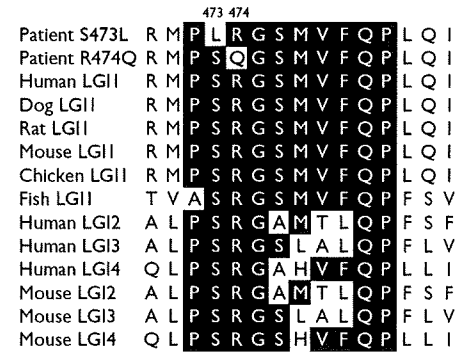

Figure 3.
Multiple amino acid sequence alignment of human LGI1 and other species. The substituted amino acids, serine at the 473rd and arginine at the 474th, are highly conserved throughout other species as well as other subtypes of LGI families.
Epilepsia © ILAE

had both GTCS and partial seizures. Auditory auras were observed in at least two members (III-3 and IV-1).

The phenotype of the family "U" was already reported in detail before the *LGI1* gene was identified as a causative gene of ADLTE in 2002 (Ikeda et al., 2000), and was relatively uniform (Fig. 2). Briefly, I-1, the father of the proband (II-3) was a 51-year-old, full-time employee with a past history of febrile convulsion. At the age of 16 years, his first nocturnal GTCS occurred. His habitual seizures also started with a high-pitched buzzing sound, followed by loss of awareness. The patient often noticed that his seizures were triggered by the telephone bell. His seizures were completely controlled after adding carbamazepine to valproic acid. Two children (II-3 was the proband in Ikeda et al., 2000) also had first GTCS and partial seizures since the second decade, and the seizures were completely controlled by carbamazepine. All of them had normal MRI, and EEG showed sharp transients in the left frontotemporal areas only in I-1, but no clear epileptiform discharges were recorded.

Gene analysis

Sequence analysis of eight exons of *LGI1* in the two patients in family "O" (IV-5 and IV-7 in Fig. 1) revealed point mutation (1418C>T, numbering from the first nucleotide of the initiator codon) resulting in amino-acid substitution of serine to leucine at the 473rd residue. Sequence analysis of DNA from the patient in family "U" (I-1 in Fig. 2) also revealed point mutation (1421G>A) resulting in amino acid substitution of arginine to glutamine at the 474th residue. Each of the two mutations disrupts the restriction enzyme site of NruI. Digesting polymerase chain reaction (PCR) product of exon 8 with NruI using buffer provided by a manufacturer (New England BioLabos, MA, U.S.A.), the two mutations were screened in control participants. There was neither 1418C>T nor 1421G>A mutation in 50 control participants, suggesting that these base changes could be regarded as mutations, but not polymorphisms.

The serine at residue 473 and arginine at residue 474 of LGI1 were highly conserved between species and its homologs, LGI2, 3, and 4 (Fig. 3). The serine at the 473rd residue was considered to be phosphorylated, and the mutation might disrupt it.

With regard to the clinical features, the reported symptoms in family "O" were consistent with previous reports of ADLTE, except that the degree and incidence of psychiatric symptoms were rather high. Symptoms in family "U" were almost common among pedigrees, except that only II-1 had déjà vu, suggestive of mesial temporal involvement. The two patients in family "O" also had déjà vu; however, other clinical features differed between them.

Discussion

Because all reported ADLTE families with *LGI1* mutations were Caucasians, we presumed that patients with *LGI1*-related epilepsy in Japan were rather rare, or that some genetic backgrounds may lower penetrance rates so that clinically they seem to be sporadic cases even though some families have *LGI1* mutations. In the present study, however, we documented that two independent families in Kyoto province had different *LGI1* mutations.

Clinical manifestations of family "O" were divided into two groups: one had seizures with auditory features and the other with psychiatric symptoms such as explosive

violent behaviors and panic attack–like symptoms. The proband also had apparently nonepileptic auditory hallucination and one member was admitted to the psychiatric hospital. The psychiatric symptoms in ADLTE were also described in the previous reports, but they were much milder. When attention was paid only to seizures with auditory features in this family, epileptic symptoms appeared after skipping two consecutive generations. Therefore, it is most likely that psychiatric symptoms are one of constellations of *LGI1*-related ADLTE. The clinical manifestations of family "O" with *S473L* mutation were different from ones of the British decedent family in Australia, even though they had a mutation identical to our patients (Berkovic et al., 2004).

On the other hand, clinical symptoms of family "U" were nearly uniform, being consistent with previously reported, typical ADLTE. Mutation at the same codon was reported in Spanish family results in premature truncation, and their clinical symptoms were also mild and had the common features of ADLTE (Morante-Redolat et al., 2002).

Recently it was reported that ADAM22 served as a receptor for LGI1, the mutated form of LGI1 failed to bind to ADAM22, and LGI1 enhances α-amino-3-hydroxy-5-methyl-4-isoxazolepropionic acid receptor–mediated synaptic transmission in rat hippocampal slices. (Fukata et al., 2006). Schulte et al. (2006) reported that LGI1 protein assembled into the presynaptic Kv1 channels and inhibited inactivation by Kvbeta1. These findings may suggest that the underlying pathogenetic mechanism of ADLTE would be "loss of function" like other numerous familial epilepsies classified into "channelopathy." However, the diversity of clinical phenotype probably depends on the mutated residue could be explained better by "gain of function" rather than "loss of function" mechanism, which would be resulting in homogenous phenotype. Further genotype–phenotype analyses in patients of different ethnic backgrounds may elucidate a part of the mechanisms.

Acknowledgment

This study was supported by the Research Grant for the Treatment of Intractable Epilepsy (19-1) from the Japan Ministry of Health, Labor and Welfare, and by the Scientific Research Grant (C2) (18590935) from the Japan Society for Promotion for Sciences (JSPS).

We confirm that we have read the Journal's position on issues involved in ethical publication and affirm that this report is consistent with those guidelines.

Disclosure: None of the authors has any conflict of interest to disclose.

References

Berkovic SF, Izzillo P, McMahon JM, Harkin LA, McIntosh AM, Phillips HA, Briellmann RS, Wallace RH, Mazarib A, Neufeld MY, Korczyn AD, Scheffer IE, Mulley JC. (2004) LGI1 mutations in temporal lobe epilepsies. *Neurology* 62:1115–1119.

Bovo G, Diani E, Bisulli F, Di Bonaventura C, Striano P, Gambardella A, Ferlazzo E, Egeo G, Mecarelli O, Elia M, Bianchi A, Bortoluzzi S, Vettori A, Aguglia U, Binelli S, De Falco A, Coppola G, Gobbi G, Sofia V, Striano S, Tinuper P, Giallonardo AT, Michelucci R, Nobile C. (2008) Analysis of LGI1 promoter sequence, PDYN and GABBR1 polymorphisms in sporadic and familial lateral temporal lobe epilepsy. *Neurosci Lett* 2008 [PMID: 18355961].

Chabrol E, Popescu C, Gourfinkel-An I, Trouillard O, Depienne C, Senechal K, Baulac M, LeGuern E, Baulac S. (2007) Two novel epilepsy-linked mutations leading to a loss of function of LGI1. *Arch Neurol* 64:217–222.

Fertig E, Lincoln A, Martinuzzi A, Mattson RH, Hisama FM. (2003) Novel LGI1 mutation in a family with autosomal dominant partial epilepsy with auditory features. *Neurology* 2003:60.

Fukata Y, Adesnik H, Iwanaga T, Bredt DS, Nicoll RA, Fukata M. (2006) Epilepsy-related ligand/receptor complex LGI1 and ADAM22 regulate synaptic transmission. *Science* 313:1792–1795.

Gu W, Brodtkorb E, Piepoli T, Finocchiaro G, Steinlein OK. (2005) LGI1: a gene involved in epileptogenesis and glioma progression? *Neurogenetics* 6:59–66.

Ikeda A, Kunieda T, Miyamoto S, Fukuyama H, Shibasaki H. (2000) Autosomal dominant temporal lobe epilepsy in a Japanese family. *J Neurol Sci* 176:162–165.

Ikeda A, Kawamata J, Matsumoto R, Takaya S, Usui K, Fukuyama H, Takahashi R. (2007) Variable clinical features in Japanese families with autosomal dominant lateral temporal lobe epilepsy ADLTLE. *Neurol Asia* 12(suppl 1):65.

Kalachikov S, Evgrafov O, Ross B, Winawer M, Barker-Cummings C, Boneschi FM, Choi C, Morozov P, Das K, Teplitskaya E, Yu A, Cayanis E, Penchaszadeh G, Kottmann AH, Pedley TA, Hauser WA, Ottman R, Gilliam TC. (2002) Mutation in LGI1 cause autosomal-dominant partial epilepsy with auditory features. *Nat Genet* 30:335–341.

Michelucci R, Poza JJ, Sofia V, de Feo MR, Binelli S, Bisulli F, Scudellaro E, Simionati B, Zimbello R, D'Orsi G, Passarelli D, Avoni P, Avanzini G, Tinuper P, Biondi R, Valle G, Mautner VF, Stephani U, Tassinari CA, Moschonas NK, Siebert R, Lopez de Munain A, Perez-Tur J, Nobile C. (2003) Autosomal dominant lateral temporal epilepsy: clinical spectrum, new epitempin mutations, and genetic heterogeneity in seven European families. *Epilepsia* 44:1289–1297.

Morante-Redolat JM, Gorostidi-Pagola A, Piquer-Sirerol S, Sáenz A, Poza JJ, Galán J, Gesk S, Sarafidou T, Mautner VF, Binelli S, Staub E, Hinzmann B, French L, Prud'homme JF, Passarelli D, Scannapieco P, Tassinari CA, Avanzini G, Martí-Massó JF, Kluwe L, Deloukas P, Moschonas NK, Michelucci R, Siebert R, Nobile C, Pérez-Tur J, López de Munain A. (2002) Mutations in the LGI1/Epitempin gene on 10q24 cause autosomal dominant lateral temporal epilepsy. *Hum Molec Genet* 11:1119–1128.

Ottman R, Risch N, Hauser WA, Pedley TA, Lee JH, Barker-Cummings C, Lustenberger A, Nagle KJ, Lee KS, Scheuer ML, Neystat M, Susser M, Wilhelmsen KC. (1995) Localization of a gene for partial epilepsy to chromosome 10q. *Nat Genet* 10:56–60.

Schulte U, Thumfart JO, Klöcker N, Sailer CA, Bildl W, Biniossek M, Dehn D, Deller T, Eble S, Abbass K, Wangler T, Knaus HG, Fakler B. (2006) The epilepsy-linked Lgi1 protein assembles into presynaptic Kv1 channels and inhibits inactivation by Kvbeta1. *Neuron* 49:697–706.

Clinical Neurophysiology 120 (2009) 1923–1926

Contents lists available at ScienceDirect

Clinical Neurophysiology

journal homepage: www.elsevier.com/locate/clinph

Abnormal auditory cortex with giant N100m signal in patients with autosomal dominant lateral temporal lobe epilepsy

Keiko Usui [a,d], Akio Ikeda [b,*], Takashi Nagamine [a], Jun Matsubayashi [a], Riki Matsumoto [b], Harukazu Hiraumi [c], Jun Kawamata [b], Masao Matsuhashi [a], Ryosuke Takahashi [b], Hidenao Fukuyama [a]

[a] Human Brain Research Center, Kyoto University Graduate School of Medicine, Kyoto, Japan
[b] Department of Neurology, Kyoto University Graduate School of Medicine, Kyoto, Japan
[c] Department of Otolaryngology, Head and Neck Surgery, Kyoto University Graduate School of Medicine, Kyoto, Japan
[d] National Epilepsy Center, Shizuoka Institute of Epilepsy and Neurological Disorders, Shizuoka, Japan

ARTICLE INFO

Article history:
Accepted 24 August 2009
Available online 29 September 2009

Keywords:
Auditory evoked magnetic fields (AEF)
MEG
Auditory aura
ADLTE
Cortical hyperexcitability

ABSTRACT

Objective: Lateralization of functionally abnormal cortical area in autosomal dominant lateral temporal lobe epilepsy (ADLTE).
Methods: A sound pulse of pure tone was delivered monaurally to the ears alternately. Auditory evoked magnetic fields (AEF) were measured by using whole-head magnetoencephalography (MEG) system.
Results: Significantly large N100m signals (a magnetic counterpart of N1/N100 in EEG) were detected in three out of five patients, either in the left or in the right hemisphere, contralateral to the auditory stimulation. The peak latency, location and orientation of distinct N100m exhibited no clear difference from those of normal controls.
Conclusions: Unilateral cortical abnormality exists in some of the patients in ADLTE. Patients with abnormally large N100m had seizures apparently provoked by auditory stimuli, suggesting that the appearance of significantly large N100m is associated with the epileptogenicity. Based on the detailed examination using MRI and FDG-PET for two of the patients, the authors hypothesize hyperexcitability caused by the decreased inhibitory functions, larger number of synchronously activated neurons, or the elongation of neuronal firing in the pathological temporal cortex in ADLTE.
Significance: The present study revealed clear abnormalities in the auditory cortex that have not been well detected by conventional EEG in patients with ADLTE.

1. Introduction

Direct evidence that the seizures originate from a specific region is obtained only when epileptic cortical activities are recorded in that particular region. Epileptic seizures usually occur sporadically and, in most cases, little neurological deficit is found during the interictal period. EEG is useful to find the abnormal cortical activities during seizures. In the interictal period, however, abnormal activities are sometimes not found in EEG. Evoked potentials (EPs) have been used to evaluate abnormality in various neurological diseases. In epileptic syndromes, it is known that somatosensory evoked potentials (SEPs) or their magnetic counterparts are extremely large in patients with progressive myoclonic epilepsy (Dawson, 1946; Watson and Denny-Brown, 1955; Halliday, 1967; Chadwick et al., 1977; Shibasaki et al., 1978; Hallett et al., 1979; Karhu et al., 1994). In other types of epilepsy, however, EPs have rarely been used to investigate latent cortical abnormality.

Autosomal dominant lateral temporal lobe epilepsy (ADLTE) is one of the rare genetic epilepsies that exhibit partial seizures (Ottman et al., 1995; Ikeda et al., 2000, 2007; Michelucci et al., 2003). Since ADLTE is characterized by recurrent auditory auras, it is assumed that the seizure onset or the irritative zone is on the lateral temporal lobe, and that the auditory cortex or its association areas are involved in the epileptic activities. Functionally abnormal cortical area, however, has not yet been clearly localized due to the fact that ictal EEG is scarcely recorded in the cases of ADLTE, and that interictal abnormality observed in EEG is also rare (Ikeda et al., 2000, 2007; Michelucci et al., 2003).

In the present study, we employed evoked magnetic field (AEF) measured by using magnetoencephalography (MEG), a magnetic version of evoked potential technique, for the investigation of interictal abnormality in the cortex in ADLTE. We investigated interictal abnormality in the cortex in ADLTE. MEG picks up

* Corresponding author. Address: Department of Neurology, Kyoto University Graduate School of Medicine, Shogoin, Sakyo-ku, Kyoto 606-8507, Japan. Tel.: +81 75 751 3772; fax: +81 75 751 9416.
E-mail address: akio@kuhp.kyoto-u.ac.jp (A. Ikeda).

1388-2457/$36.00
doi:10.1016/j.clinph.2009.08.020

cortical activities right beneath the magnetic sensors with high spatial and temporal resolutions, and thus enabled us to evaluate the cortical function of the left and right temporal lobes separately (Hari, 1990). The content of this paper did not appear elsewhere except for an abstract (Ikeda et al., 2007)

1.1. Subjects and methods

1.1.1. Subjects

Five right-handed patients from three families with ADLTE participated in the present study. Table 1 shows their clinical profile. The clinical details of the patients, have been reported elsewhere (Ikeda et al., 2000, 2007; Kawamata et al., in press; Fujita et al., 2009). Families U and O were genetically diagnosed as ADLTE (Ikeda et al., 2007; Kawamata et al., in press; Fujita et al., 2009). All patients had auditory auras and three of them (Patients 2, 4 and 5) had seizures triggered by specific sound. In interictal period, no neurological deficits and hearing disturbance were observed. In all patient EEG showed no definite epileptic discharges in interictal period.

3-Tesla or 1.5-Tesla MR images were taken in all patients. MRI showed volume reduction in unilateral temporal lobe in two patients (Patients 4 and 5) and the left hippocampal sclerosis in one patient (Patient 3). [F-18]fluorodeoxyglucose-positron emission tomography (FDG-PET) showed glucose-hypometabolism in the same temporal lobes with MRI abnormality in Patients 3, 4 and 5.

Ten healthy volunteers (2 females) of the age between 20 and 43 y.o. (mean (SD), 30.9(6.1)) with no neurological deficits and hearing disturbance were recruited in the study as normal control. All the procedures were approved by Kyoto University Graduate School and Faculty of Medicine, Ethics Committee and written informed consent was obtained from all patients and normal volunteers.

1.1.2. MEG measurement and analysis

AEFs were measured by using a 306-channel whole-head system (VectorView, Elekta Neuromag, Finland). It was confirmed that the patients with ADLTE had no seizures within 12 hours before the AEF recording. No seizure occurred during the recording. A sound pulse of pure tone of 1000 Hz was delivered through ear tubes monaurally to the right and left ears alternately. Level of the sound pulses was controlled so that both patients and normal volunteers were given auditory stimuli at SL (sensation level) of 50 dB above his or her hearing threshold. Output of the sound pulse generator was individually set at SL (sensation level) of 50 dB above the hearing threshold of each subject or normal controls. The duration of the pulse was 130 ms (the rise and fall time of 10 ms each) with 1000 ± 70-ms intervals.

MEG were recorded with bandpass filter of 0.1–330 Hz and with sampling rate of 997 Hz. Epochs for on-line averaging started 100 ms before the onset of each stimuli and terminated 400 ms after the onset. Each stimulus given to the right or left ear were averaged separately. Epochs containing blinks and/or other artifacts were automatically excluded from averaging. More than 100 epochs for each right- and left ear stimulation were averaged in one measurement. Two or three measurements were performed in each subject in order to confirm that auditory magnetic responses were reproduced.

N100m, a magnetic counterpart of N1/N100 in EEG, which is the most prominent component of AEFs (Pantev et al., 1995; Lutkenhoner and Steinstrater, 1998), were analyzed. The activated brain areas were modeled as equivalent current dipoles (ECDs) (Hamalainen et al., 1993). A spherical model, which is made from each subject's anatomical 0.5-Tesla 3-dimensional MR images (Signa, General Electric, USA), was used for describing the conductivity profile of the brain. The ECDs were estimated from at least 27 channels (= 9 set of sensors), that covered the field pattern of 100 ms component in auditory magnetic fields over each hemisphere. The ECDs with goodness of fit (GOF) more than 80% and confidence volume (CV) less than 1000 mm^3 were used for further analysis.

The mean and standard deviation (SD) of ECD moment and peak latency of N100m were obtained from the control subjects. The data of patients and of control group were compared, and the values that surpassed the mean + 2.5 SD of those obtained from control group were regarded as significantly large.

2. Results

Fig. 1 shows representative magnetic responses of a patient (Patient 4) to the auditory stimuli given to the left and right ears. Shown in this figure are waveforms in 306 channels (A and D), largest responses detected by planar gradiometer in the contralateral hemisphere to the stimuli (insets of A and D), magnetic field maps and estimated ECDs at 97 ms from stimulus onset in the contralateral hemisphere (B and E), and the ECDs superimposed on the patient's anatomical MR images (C and F). The latency and estimated ECD moment (strength) of N100m peak in each patient are shown in Table 2 in comparison with the mean (SD) of those in normal controls. In all patients, the peak latency of N100m showed no significant difference from those of the control group. The sources of N100m were localized in the temporal plane in each hemisphere of both patients and control subjects, and no significant difference in the location and orientation of sources was identified.

As for the ECD moment, significantly large response was recorded in three patients either in the left (Patients 2 and 4) or in the right (Patient 5) hemisphere, contralateral to the auditory

Table 1
Clinical profile of patients with ADLTE.

Patient	Age	Sex	Family	Types of aura	Seizure types	Inducing factors of seizures	Findings in MRI and/or FDG-PET
1	31	M	U	Auditory, deja vu	SPS, CPS, *n*-GTCS	None	No abnormal findings
2	56	M	U	Auditory	SPS, CPS, *n*-GTCS	Ringing of phone	No abnormal findings
3	27	F	U	Auditory	SPS, CPS, *n*-GTCS	None	Left hippocampus: sclerosis suspected Left temporal lobe: mild hypometabolism suspected
4	27	F	O	Auditory, deja vu	SPS, CPS	Specific sound, conversation	Left superior temporal gyrus: small in volume Left temporal lobe: hypometabolism
5	36	F	H	Auditory, deja vu	SPS, CPS	Specific music	Right inferior horn of lateral ventricle: enlargement Right temporal lobe: hypometabolism

SPS, simple partial seizures; CPS, complex partial seizures; *n*-GTCS, nocturnal generalized tonic–clonic seizures.

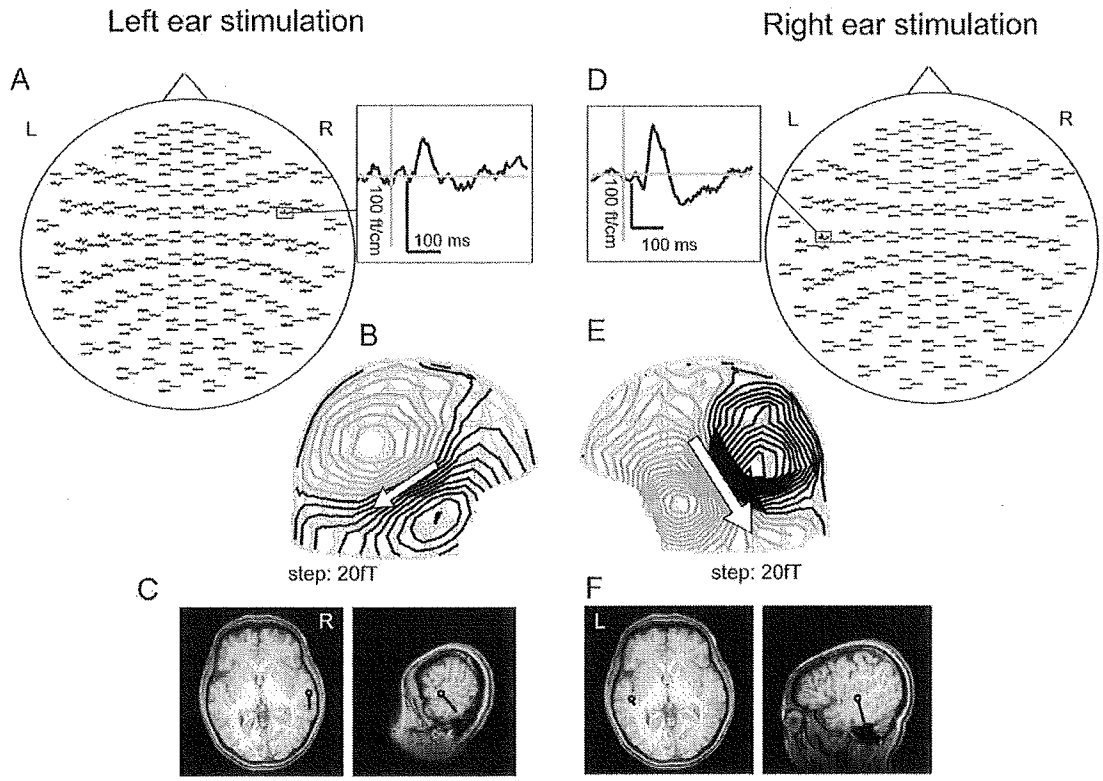

Fig. 1. Auditory evoked magnetic fields of Patient 4. Magnetic responses to the left ear stimulation are shown in the left and the responses to the right ear stimulation in the right. Upper panels (A and D) show responses in all channels. The traces show a 500 ms time period starting 100 ms before the stimulus onset. The insets show the magnified largest responses in the contralateral hemisphere to the stimuli. Lower panels show field map and ECD of N100m. Field patterns in the contralateral hemisphere to the stimuli at the peak latency (97 ms from stimulus onset) are shown in panels (B) and (E). The maps were drawn over the helmet-shaped sensor array. The step between the isocontour lines is 20 fT. The areas with black lines indicate the magnetic field out of the head and the areas with gray lines indicate the field into the head. The arrows show the estimated location of the ECDs projected onto the subject's head surface. Panels (C) and (F) show the ECD location superimposed on the subject's 3-dimensional MR images.

Table 2
Peak latency and ECD moment of N100m in the contralateral and ipsilateral hemispheres to unilateral auditory stimuli.

Subject	Lt ear stimulation				Rt ear stimlation			
	Contralateral (Rt)		Ipsilateral (Lt)		Contralateral (Lt)		Ipsilateral (Rt)	
	Latency (ms)	Moment (nAm)	Latency (ms)	Moment (nAm)	Latency (ms)	Moment (nAm)	Latency (ms)	Moment (nAm)
P1	98	40.8	112	13.0	103	12.2	108	27.5
P2	106	51.2	127	37.7*	114	88.0*	114	45.5
P3	94	21.2	104	13.8	98	17.7	118	24.8
P4	97	18.5	96	30.6	97	44.2*	104	13.1
P5	97	83.7*	111	7.6	105	15.8	114	42.3
Control	Latency(SD)	Moment(SD)	Latency(SD)	Moment(SD)	Latency(SD)	Moment(SD)	Latency(SD)	Moment(SD)
(n = 10)	97.3 (5.7)	35.4 (14.1)	108.9 (11.8)	18.5 (6.6)	98.2 (10.5)	23.6 (7.3)	105.7 (8.6)	27.5 (12.0)

P, patient; Lt, left; Rt, right. The data of control group are shown as the mean (SD).
* >The mean + 2.5 SD of control group.

stimulation. In the left hemispheres of Patients 2 and 4 and the right hemisphere of Patient 5, large N100m was also evoked in response to the ipsilateral stimuli and the ECD moment was significantly large for Patient 2. In the remaining patients (Patients 1 and 3) the ECD moment of N100m was not different from those of the control group.

3. Discussion

Morphological and/or functional abnormality in ADLTE has been reported predominantly on the left hemisphere in the literature so far. In one study, for example, it was reported that morphological abnormality lateralized on the left hemisphere existed in 45% of 22 patients with ADLTE (Kobayashi et al., 2003). Another study reported abnormality in auditory evoked potentials (AEPs) lateralized on the left (Brodtkorb et al., 2005).

Epileptogenicity and functional deficit, however, are caused not only by visually detectable malformations but also by some other abnormalities. In addition, AEP evaluation using EEG and binaural sound presentation are not appropriate to distinguish left and right auditory responses separately. It is, therefore, uncertain how much the causes of ADLTE is associated with morphological abnormality that is localized on the left hemisphere.

In this study using AEF, ECD moment of N100m can be classified into two groups: one with the values larger than +2.5 SD, and the other with the values smaller than +2.5 SD. For brevity, we call the former "large signal" and the latter "small signal". N100m

signals of three patients were clearly larger than those of other patients. The results of these three exhibit unique features that should be mentioned. First noticeable feature is that these larger signals were observed in the left hemisphere for two patients and in the right for the other patient.

Second noticeable and striking feature is that the N100m in the right hemisphere of the two patients who exhibited large signals in the left was small. It is also found that the N100m in the left hemisphere of the other patient who exhibited large signal in the right was small. The fact that the significantly large N100m signals were detected in either left or right hemisphere in three patients, and that the N100m in the opposite hemisphere of all these three patients were small is a clear indication that unilateral cortical abnormality exists, at least in some patients, in ADLTE.

Third noticeable feature is that, as compared with the normal subjects, the latency of large N100m showed no distinct difference in the case of ADLTE patients. This result strongly suggests that no disturbance in both peripheral and central auditory pathways.

Fourth feature is that, although the ECD moment of N100m was distinctively large in the patients, the location and orientation was similar to those in control subjects. The similar location and orientation of the ECD suggested that the center of neuronal populations underlying N100m response are supposed to be the same, or, at least, very close in the giant and normal AEFs. (For detailed mechanism see Eggermont and Ponton, 2002 and references therein)

Further detailed examination for two of the patients using MRI and FDG-PET showed the anatomical and functional deficit localized in the temporal lobes. The volume of the temporal lobe which generated the giant N100m was reduced (possibly due to malformation or atrophy) and glucose-hypometabolism was detected. Volume reduction and hypometabolism usually suggest cortical hypofunction, which is supposed to lead weak signals. The two patients with ADLTE, whose cortical area was reduced in volume, by contrast, generated larger N100m than those with cortices of normal volume.

Since there is no way to reveal the underlying mechanism of the distinctively large ECD moment or the strength of MEG response with concrete experimental evidence in our study so far, we present the hypotheses. One possible explanation is the hyperexcitability of the neurons: the amount of the neurons is the same but the neurons of the patients are hyperreactive. If the neuronal population producing N100m is hyperexcited, the signals would be apparently larger than those of normal activity. Large dipole moment may also indicate highly coordinated activity. If the amount of synchronously activated neurons is larger in the patients with ADLTE than in the normal controls, the signals would be apparently larger. Other possible explanation may be the elongation of neuronal firing. To clearly distinguish the factors affecting the N100m signal, microscopic invasive study using depth or subdural electrodes is needed.

Our investigation found that three patients exhibited distinctively large N100m and the remaining two patients exhibited comparatively small N100m. The difference observed between two groups of patients was that the former had seizures apparently provoked by auditory stimuli, such as specific sound or music, while the latter did not. These facts suggest that the appearance of significantly large N100m in the auditory cortex, which indicates abnormally large response to sound, may be closely associated with the epileptogenicity in these patients, just as giant SEPs in patients with progressive myoclonic epilepsy.

In summary, the present study using auditory magnetic fields showed that significantly large N100m signals are supposed to be an indication of auditory induced seizures. Our result is also a clear demonstration of significant usefulness of AEF in the detailed studies to address the issue of whether unilateral or bilateral temporal lobes are involved. This technique enables these evaluations even for the interictal period.

Conflict of interest

The authors have no financial conflicts to report.

Acknowledgement

This study was supported by the Research Grant for The Treatment of Intractable Epilepsy (19-1) from the Japan Ministry of Health, Labor and Welfare, the Scientific Research Grant (C2) (18590935) from the Japan Society for Promotion of Sciences (JSPS) and the Grant-in-Aid for Scientific Research on Priority Areas (20020013) from the Ministry of Education, Culture, Sports, Science and Technology (MEXT).

References

Brodtkorb E, Steinlein OK, Sand T. Asymmetry of long-latency auditory evoked potentials in LGI1-related autosomal dominant lateral temporal lobe epilepsy. Epilepsia 2005;46:1692–4.

Chadwick D, Hallett M, Harris R, Jenner P, Reynolds EH, Marsden CD. Clinical, biochemical and physiological features distinguishing myoclonus responsive to 5-hydroxytryptophan, tryptophan with a monoamine oxidase inhibitor, and clonazepam. Brain 1977;100:455–87.

Dawson GD. The relation between the electroencephalogram and muscle action potentials in certain convulsive states. J Neurol Neurosurg Psychiatry 1946;10:141–62.

Eggermont JJ, Ponton CW. The neurophysiology of auditory perception: From single units to evoked potentials [review]. Audiol Neurootol 2002;7:71–99.

Fujita Y, Ikeda A, Kadono K, Kawamata J, Tomimoto H, Fukuyama H, Takahashi R. Clinical features in a Japanese patient with autosomal dominant temporal lobe epilepsy having *LGI1* mutation. Clin Neurol (Tokyo) 2009;49:186–90 [in Japanese].

Hallett M, Chadwick D, Marsden CD. Cortical reflex myoclonus. Neurology 1979;29:1107–25.

Halliday AM. The neurophysiological study of myoclonus in man. Brain 1967;90:241–84.

Hamalainen M, Hari R, Ilmoniemi RJ, Knuutila J, Lounasmaa OV. Magnetoencephalography-theory, instrumentation, and applications to noninvasive studies of the working human brain. Rev Modern Phys 1993;65:413–97.

Hari R. The neuromagnetic method in the study of the human auditory cortex. In: Grandori F, Hoke M, Romani G, editors. Auditory evoked magnetic fields and electric potentials. Advances in audiology 1990;vol. 6. Basel: Karger; 1990. p. 222–82.

Ikeda A, Kunieda T, Miyamoto S, Fukuyama H, Shibasaki H. Autosomal dominant temporal lobe epilepsy in a Japanese family. J Neurol Sci 2000;176:162–5.

Ikeda A, Kawamata J, Matsumoto R, Takaya S, Usui K, Fukuyama H, et al. Variable clinical features in Japanese families with autosomal dominant lateral temporal lobe epilepsy (ADLTLE). Neurol Asia 2007;12(Suppl. 1):65 [abstract].

Karhu J, Hari R, Paetau R, Kajola M, Mervaala E. Cortical reactivity in progressive myoclonus epilepsy. Electroencephalogr Clin Neurophysiol 1994;90:93–102.

Kawamata J, Ikeda A, Fujita Y, Usui K, Shimohama S, Takahashi R. Mutation in *LGI1* gene in Japanese Families with autosomal dominant lateral temporal lobe epilepsy: the first report from Asian families. Epilepsia, in press.

Kobayashi E, Santos NF, Torres FR, Secolin R, Sardinha LAC, Lopez-Cendes I, Cendes F. Magnetic resonance imaging abnormalities in familial temporal lobe epilepsy with auditory auras. Arch Neurol 2003;60:1546–51.

Lutkenhoner B, Steinstrater O. High-precision neuromagnetic study of the functional organization of the human auditory cortex. Audiol Neurootol 1998;3:191–213.

Michelucci R, Poza JJ, Sofia V, de Feo MR, Binelli S, Bisulli F, et al. Autosomal dominant lateral temporal epilepsy: clinical spectrum, new epitempin mutations, and genetic heterogeneity in seven European families. Epilepsia 2003;44:1289–97.

Ottman R, Risch N, Hauser WA, Pedley TA, Lee JH, Barker-Cummings C, et al. Localization of a gene for partial epilepsy to chromosome 10q. Nat Genet 1995;10:56–60.

Pantev C, Bertrand O, Eulitz C, Verkindt C, Hampson S, Schiuierer G, Elbert T. Specific tonotopic organizations of different areas of the human auditory cortex revealed by simultaneous magnetic and electric recordings. Electroencephalogr Clin Neurophysiol 1995;94:26–40.

Shibasaki H, Yamashita Y, Kuroiwa Y. Electroencephalographic studies of myoclonus: myoclonus-related cortical spikes and high amplitude somatosensory evoked potentials. Brain 1978;101:447–60.

Watson CW, Denny-Brown D. Studies of the mechanism of stimulus-sensitive myoclonus in man. Electroencephalogr Clin Nueophysiol 1955;7:341–56.

J Neuropathol Exp Neurol

Vol. 68, No. 10
October 2009
pp. 1084–1091

ORIGINAL ARTICLE

Selective Nuclear Shrinkage of Oligodendrocytes Lacking Glial Cytoplasmic Inclusions in Multiple System Atrophy: A 3-Dimensional Volumetric Study

Naoto Uyama, MD, Toshiki Uchihara, MD, PhD, Yoko Mochizuki, MD, PhD, Ayako Nakamura, Ryosuke Takahashi, MD, PhD, and Toshio Mizutani, MD, PhD

Abstract

Glial cytoplasmic inclusions (GCIs) are a pathologic hallmark of multiple system atrophy (MSA), but their pathogenetic roles need to be clarified. To determine possible roles of GCIs in individual cells, serial optical sections obtained by confocal microscopy were reconstructed to yield 3-dimensional (3D) images of the nuclei to quantify nuclear volume. Oligodendroglial nuclear volumes were determined in the pons of 6 MSA and 7 control patients. The nuclear volumes were significantly smaller in the MSA group as a whole (135.81 ± 60.83 μm^3, mean ± SD; n = 404) than in the control group (188.05 ± 55.71 μm^3; n = 308; $p < 0.001$). This difference was due to a significantly smaller nuclear volume of oligodendrocytes without GCIs (GCI^- group, 91.26 ± 23.77 μm^3; n = 210) compared with the control group ($p < 0.001$) and compared with the oligodendrocytes with GCIs (GCI^+ group, 184.03 ± 51.18 μm^3; n = 194; $p < 0.001$); the difference between the latter GCI^+ and control groups was not significant ($p > 0.05$). This selective decrease in nuclear volume restricted to the GCI^- group cannot be explained if nuclear shrinkage was accelerated in the presence of GCIs. Conversely, GCI formation might be linked, either directly or indirectly, to a mechanism that counteracts rather than accelerates nuclear shrinkage. This novel 3-dimensional strategy provides pivotal data that link GCI formation and degeneration in MSA.

Key Words: Glial cytoplasmic inclusions, Multiple system atrophy, Nuclear volume, Three-dimensional reconstruction.

INTRODUCTION

Multiple system atrophy (MSA) (1) is characterized by the distribution of degenerative lesions and the presence of glial cytoplasmic inclusions (GCIs) (2, 3). Because GCIs are a pathologic hallmark of MSA, they are believed to be tightly linked to the pathogenic mechanism of MSA; numerous studies have attempted to clarify possible relationships between the presence of GCIs and the extent and severity of degeneration (4–7). Reported data are, however, highly variable, and none of the previous neuropathologic studies have established a pathogenetic role for GCIs. Although it has been reported that nuclei of GCI-bearing oligodendrocytes (GCI^+) usually appear larger than those of oligodendrocytes that do not harbor GCIs (GCI^-) (8, 9), it is unclear whether the presence of GCIs is linked to accelerated neurodegeneration. Because the degenerative cascade of MSA leads both to GCI formation and cellular degeneration, the morphologic parameters (e.g. nuclear volume) of an individual oligodendrocyte might be influenced by the formation of GCIs. In this study, we focus on the nuclear volume of oligodendrocytes with or without GCIs. Instead of using conventional indirect methods of volume estimation (10–12), we measured the actual nuclear volume of each oligodendrocyte reconstructed into a 3-dimensional (3D) image from serial optical sections (~200 sections at an interval of 0.1 μm) spanning the entire oligodendrocyte. This straightforward method has been used mainly in the field of diagnostic radiology and provides estimates of the real volume regardless of the shape of the targets (13–15) and is readily applicable to serial data obtained with confocal microscopy (16). This is the first successful attempt to measure directly the actual nuclear volume of oligodendrocytes. Because a decrease in nuclear volume relative to the control was significant only in GCI^- oligodendrocytes but not in GCI^+ oligodendrocytes, it is possible to conclude that nuclear shrinkage is accelerated in the absence of GCIs.

MATERIALS AND METHODS

Six patients with the clinical and neuropathologic diagnosis of MSA (3 men, 3 women; age range at death, 54–74 years) autopsied at the Department of Pathology, Tokyo Metropolitan Neurological Hospital, Tokyo, Japan, and 7 control patients (6 men, 1 women, age range at death, 47–84 years) with no

From the Department of Neurology (NU, TU, AN), Tokyo Metropolitan Institute for Neuroscience, Tokyo; the Departments of Neurology (NU) and Pathology (YM, TM), Tokyo Metropolitan Neurological Hospital, Tokyo; and the Department of Neurology (NU, RT), Kyoto University, Kyoto, Japan.

Send correspondence and reprint requests to: Toshiki Uchihara, MD, PhD, Department of Neurology, Tokyo Metropolitan Institute for Neuroscience, 2-6 Musashi-dai, Fuchu, Tokyo 183-8526, Japan; E-mail: uchihara-ts@igakuken.or.jp

This study was supported by a research grant from the Tokyo Metropolitan Organization for Medical Research to the Three Dimension Project (Neurology).

Supplemental digital content is available for this article. Direct URL citations appear in the printed text and are provided in the HTML and PDF versions of this article on the journal's Web site (www.jneuropath.com).

TABLE 1. Demographic Features of Patients With MSA and Controls

Case	Age of Onset/Death, Years	Sex*	Cause of Death	Brain Weight, g
MSA 1	47/54	F	Sudden death	1,310
MSA 2	51/58	M	Pneumonia	1,318
MSA 3	52/59	F	Pulmonary insufficiency	1,230
MSA 4	57/61	F	Pulmonary insufficiency	1,296
MSA 5	63/69	M	Cardiac insufficiency	1,225
MSA 6	70/74	M	Pulmonary insufficiency	1,285
Mean ± SD	56.7 ± 8.5/62.5 ± 7.5†			1,277.3 ± 40.3‡
Control 1	/47	M	Guillan-Barré syndrome	1,390
Control 2	/67	F	Thymic anaplastic carcinoma	1,222
Control 3	/73	M	Crow-Fukase syndrome	1,390
Control 4	/73	M	Acute myocardial infarct	1,320
Control 5	/81	M	Chronic constrictive pericarditis	1,282
Control 6	/76	M	CIDP	1,215
Control 7	/84	M	Aortic dissection	1,225
Mean ± SD	/71.6 ± 12.2			1,292.0 ± 76.8

*No significant difference between control and MSA groups (by Fisher exact test).
†$p > 0.05$ compared with control group (by Student *t*-test).
‡$p > 0.05$ compared with control group (by Student *t*-test).
CIDP, chronic inflammatory demyelinating polyradiculoneuropathy; F, female; M, male; MSA, multiple system atrophy.

disease involving the central nervous system were studied. The durations of MSA ranged from 4 to 7 years (Table 1). The diagnosis of MSA was confirmed postmortem on the basis of neuronal loss and the presence of GCIs in relevant regions, including the putamen, cerebellar white matter, and motor cortex (4). Oligodendrocytes in pontine transverse fibers were chosen for analysis because the size and appearance of oligodendroglial nuclei were relatively homogeneous, which made it easier to quantify and interpret their morphologic changes. Moreover, the high frequency of GCIs in the pons of MSA brains is another advantage in estimating their possible effects.

Formalin-fixed blocks were obtained from the midpons of MSA and control brains, washed in 0.1 mol/L phosphate buffer 3 times, then kept in 15% sucrose/0.1 mol/L phosphate buffer solution until they sank. Free-floating sections 30 μm thick were prepared on a freezing microtome and kept at 4°C until use. These sections were pretreated with 99% formic acid for 5 minutes at room temperature. The sections were blocked with 5% normal goat serum and incubated for 6 days or more at 4°C (17) with a polyclonal rabbit anti-human ubiquitin (Z0458, 1:100, DakoCytomation, Glostrup, Denmark) diluted in 0.01 mol/L PBS containing 0.3% Triton X-100 and 5% normal goat serum. The sections were washed with PBS containing 0.3% Triton X-100 3 times for 10 minutes each between steps of the entire procedure. The sections were then incubated with a polyclonal goat anti-rabbit immunoglobulin G conjugated with Alexa Fluor 546 (1:200; Molecular Probes, Eugene, OR) for 4 hours at room temperature. The sections were then immersed in 0.01 mol/L PBS containing 4′,6-diamidino-2-phenylindole, dihydrochloride (D1306, 1:1500; Molecular Probes) for 5 minutes. After washing, they were mounted with buffered glycerol containing *p*-phenylenediamine to minimize photobleaching. The sections were observed under a fluorescence microscope equipped with a laser confocal system (FV-1000; Olympus, Tokyo, Japan). At least 20 oligodendroglial nuclei from each case were selected randomly by encompassing the entire pontine nucleus; 308 were counted in the control group, 194 in the GCI^+ group and 210 in the GCI^- group (Table 2). Oligodendroglial nuclei were identified based on their round and small morphology with a linear alignment in the stretch of 5 to 10 contiguous oligodendrocytes along the long axis of nerve fibers. Larger nuclei of astrocytes or small angular nuclei of microglia (18) (both not in linear alignment) were easily distinguishable. Only cells with round nuclei serially lined in proximity (within twice the diameter of nuclei) along transverse fibers and with comparatively uniform size in the stretches were identified as

TABLE 2. Nuclear Volume of Oligodendroglia in MSA and Control Cases

	Control Cases, n = 7	Total Oligodendrocytes in MSA Cases, n = 6	Oligodendrocytes in MSA Cases With GCI	Oligodendrocytes in MSA Cases Without GCI
No. oligodendrocytes evaluated	308	404	194	210
Oligodendrocyte Volume (mean ± SD), μm^3	188.05 ± 55.71	135.81 ± 60.83*	184.03 ± 51.18‡	91.26 ± 23.77†§

*$p < 0.001$ compared with control group (by Mann-Whitney U test [Bonferroni correction]).
†$p < 0.001$ compared with control group (by 1-way analysis of variance [ANOVA]).
‡No significant difference compared with control group (by 1-way ANOVA).
§$p < 0.001$ compared with GCI^+ group (by 1-way ANOVA).
GCI, glial cytoplasmic inclusion; MSA multiple system atrophy.

oligodendrocytes. Serial optical sections at an interval of 0.1 μm were obtained to encompass the entire structure of each oligodendrocyte. Usually, 200 serial optical sections were sufficient to encompass the entire structure of an oligodendrocyte, including GCIs when they were present. Each 3D image data set consisted of a series of 2-dimensional (2D) images (Fig. 1 and Video, Supplemental Digital Content 1, http://links.lww.com/NEN/A60). Each image frame had a 63.5-μm field of view with a 512 × 512-pixel array, yielding 0.124 × 0.124-μm/pixel dimensions. The data were reconstructed for 3D observation and quantification by using software (TRI/3D SRFII-64 Release 4, Ratoc, Tokyo, Japan) running on the Windows platform on a 64-bit basis. To estimate nuclear volume with this software, the 2D contour of each nucleus, along the nuclear membrane labeled with 4′,6-diamidino-2-phenylindole, dihydrochloride, was traced manually on some of the 2D images every 4 to 5 images. The relative position of the manually defined contour and the fluorescence intensity of 4′,6-diamidino-2-phenylindole, dihydrochloride were used to calculate automatically the nuclear contour in intervening optical sections; these were later confirmed by inspection. This yielded the binary representation of the nuclear contour of an oligodendrocyte on a 3D basis consisting of noncubic voxels (0.124 × 0.124 × 0.1 μm). Subsequently, after discarding spurious voxels from the binary oligodendroglial nucleus representation, these data sets were reconstructed for 3D observation and quantification (Video, Supplemental Digital Content 2, http://links.lww.com/NEN/A61), and the total number of voxels, which substitute the nucleus, was obtained on the basis of a known voxel size of 0.0015376 μm^3, yielding the actual volume size (13–16).

Statistical analyses were performed using Dr. SPSSII for Windows software (SPSS Japan, Tokyo, Japan). Size distributions according to nuclear volume were estimated by the Kolmogorov-Smirnov method to determine whether they were compatible with the normal distribution in each patient or group (control, MSA total [GCI^+ and GCI^-], GCI^+, GCI^-). Because the size distribution of the MSA total group did not exhibit normality, its comparison with that of the control group was estimated using the Mann-Whitney U test with Bonferroni correction. Otherwise, the 1-way analysis of variance (ANOVA) was used to compare nuclear volume among the different groups when nuclear sizes exhibited a normal distribution.

RESULTS

There were no significant differences among groups with respect to age or brain weight (by Student *t*-test) or sex (by Fisher exact test; Table 1). The nuclear volume size distributions are shown in Table 2 and Figures 2 and 3. Because the size distributions showed normal distributions (as determined by the Kolmogorov-Smirnov test when each patient or each group was analyzed), our sampling and volumetric analysis procedure yielded data representative of a homogenous cell group not only in each patient but also in each group. The quantile-quantile plots of data of the GCI^+, GCI^-, and control groups show almost linear distributions

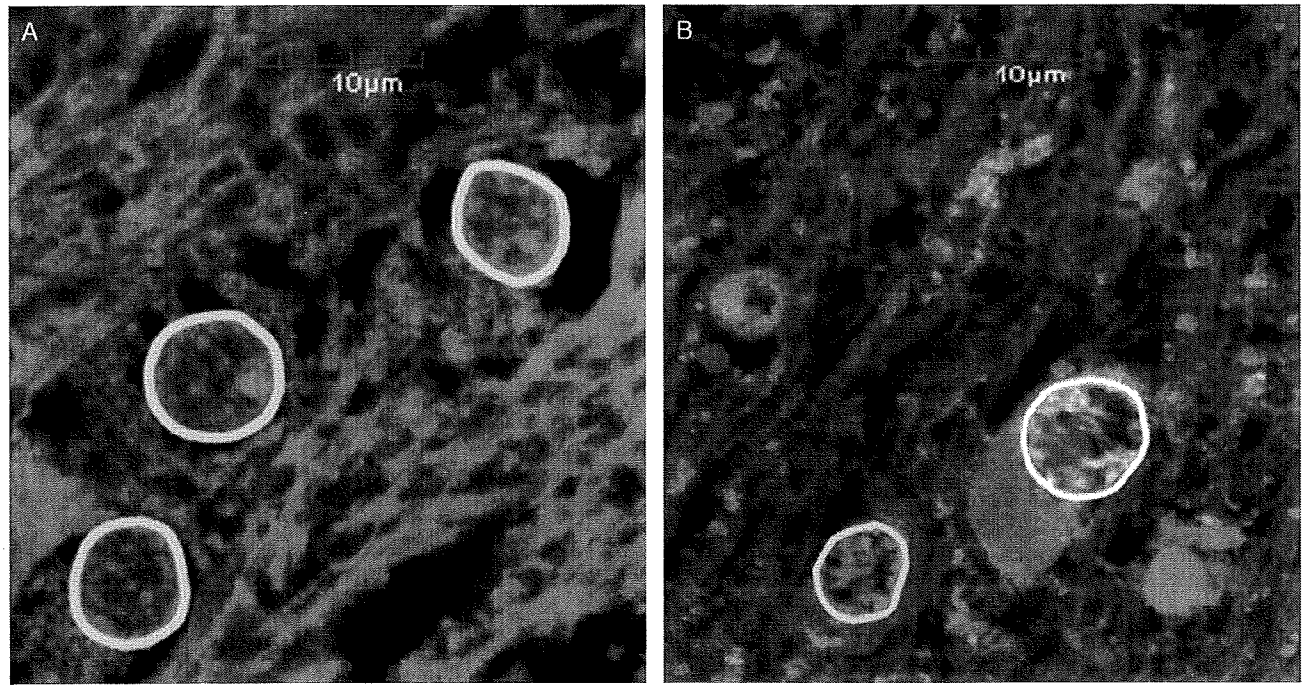

FIGURE 1. Pontine oligodendrocytes in control and MSA patients. **(A)** Oligodendrocytes in a control patient. DAPI stain (light blue). **(B)** Oligodendrocytes in an MSA patient. Double-fluorescence labeling for DAPI and ubiquitin (red). The contours of the nucleus of each oligodendrocyte are traced in yellow (oligodendrocytes without glial cytoplasmic inclusions [GCIs]) and in white (oligodendrocyte with GCIs in **B**). Bar = 10 μm. DAPI, 4′,6-diamidino-2-phenylindole, dihydrochloride.

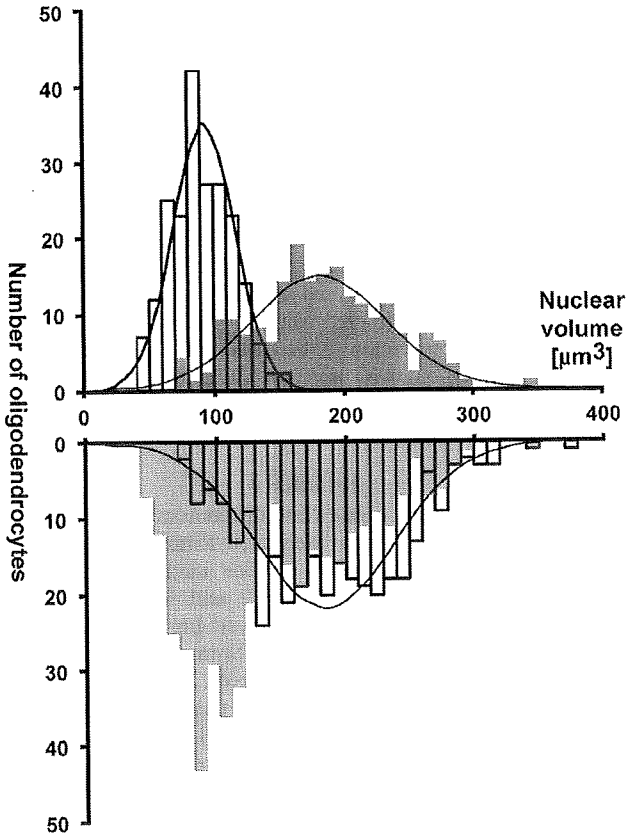

FIGURE 2. Histograms of size distribution of oligodendroglial nuclei. The nuclear volumes in cubic microns are expressed on the abscissa. The ordinate represents the relative frequency of calculated nuclear size. The lower inverted histograms represent the controls (unfilled bars with black lines) and the multiple system atrophy (MSA) group as a whole (MSA total group, bars filled with gray); the latter shows neither unimodal (single peak) nor bimodal (double peak) curves. The upper histograms indicate the MSA group with glial cytoplasmic inclusions (GCIs) (GCI^+ group, bars filled with gray) or without GCIs (GCI^- group, unfilled bars with black lines).

along the lines representing the normal distribution (Fig. 4). Although the control group exhibited a normal size distribution with a single peak, the data from the MSA total group (consisting of GCI^+ and GCI^- groups) were not in a normal distribution. The nuclear volumes were significantly smaller in the MSA total group (135.81 ± 60.83 μm^3; mean ± SD; n = 404) compared with the control group (188.05 ± 55.71 μm^3; n = 308; $p < 0.001$ by the Mann-Whitney U test with Bonferroni correction). This difference was due to the significantly smaller nuclear volume of the GCI^- group (91.26 ± 23.77 μm^3; n = 210) compared with the control group ($p < 0.001$ by 1-way ANOVA) and compared with the MSA GCI^+ group (184.03 ± 51.18 μm^3; n = 194; $p < 0.001$ by 1-way ANOVA). The nuclear volume of the GCI^+ group was not significantly different from that of the control group ($p > 0.05$ by 1-way ANOVA). Moreover, the nuclear volume of the GCI^+ group was significantly larger than that of the GCI^- group ($p < 0.001$ by 1-way ANOVA). Thus, there was a selective decrease in nuclear volume that was restricted to the GCI^- group.

DISCUSSION

This is the first study to demonstrate a decrease in the actual nuclear volume of oligodendrocytes in the pons in MSA. This volume decrease was due to the smaller nuclear volume of GCI^- than of the control, whereas the nuclear volume of GCI^+ was equivalent to that of the control. The technical novelty of this study includes 3D reconstruction of target structures (nuclei), followed by direct quantification of the entire structures.

Routine evaluation of histologic sections is usually performed on 2D basis on thin-sample specimens in which cell loss is perceived as a decrease in local density and atrophy as the volume loss of the cell body. One-dimensional indices such as diameter and perimeter are ready candidates for representing structure sizes, but sophisticated 2D indices such as cross-sectional area of the structures allow more precise determinations of their size. Using 2D quantification of neuronal size in the substantia nigra, Ma et al (19) demonstrated a 3.2% decrease per decade, whereas Cruz-Sánchez et al (20) reported progressive swelling with aging by simple comparisons of images. Similar discrepancies

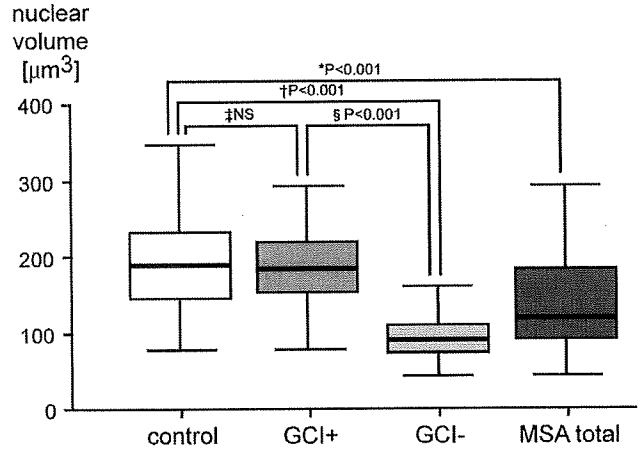

FIGURE 3. Comparison of size distribution of oligodendroglial nuclei from each group. Box plots show the nuclear volumes for each group (control; glial cytoplasmic inclusion $[GCI]^+$, oligodendrocytes with GCIs from multiple system atrophy [MSA] cases; GCI^-, oligodendrocytes without GCIs from MSA cases, MSA total, all oligodendrocytes from MSA cases). The boxes enclose the middle half of the values bounded by upper and lower quartiles. The bold lines represent the medians. The lower whisker indicates the smallest nonoutlier observation; the upper whisker indicates the nonoutlier observation. *, $p < 0.001$ when compared with control group (by the Mann-Whitney U test; Bonferroni correction); †, $p < 0.001$ when compared with control group (by 1-way analysis of variance [ANOVA]); ‡, NS, no significant difference when compared with control group (by 1-way ANOVA); §, $p < 0.001$ when compared with GCI^+ group (by 1-way ANOVA).

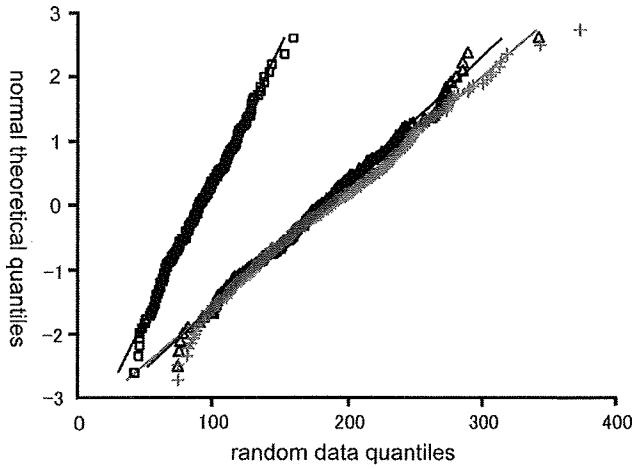

FIGURE 4. Normal distribution of nuclear volumes. The Q-Q plot shows the comparison of the distribution of a given variable with the normal distribution (represented by straight lines). The straight lines represent what the data would look like if they were normally distributed. The actual data are represented by the symbols plotted along this line; the closer the points are to the line, the more normally distributed the data appear. Most of the data points fall almost perfectly along the line, indicating that the data are normally distributed. Oligodendrocytes with glial cytoplasmic inclusions (GCI^+), open triangles; oligodendrocytes without GCIs (GCI^-) in multiple system atrophy (MSA), open squares; control, gray crosses. Q-Q, quantile-quantile.

among the studies have also been observed in Parkinson disease (21, 22), suggesting that 2D representation of 3D reality into a single plane is not sufficient.

Various stereologic methods have been developed by synthesizing 2D data sets to estimate volumes (10–12). These methods essentially include 2 steps: theoretically unbiased sampling of 2D raw data set and virtual estimation of the volume. Although still indirect, these innovative strategies made it possible to estimate the volume on a 3D basis. Even with these 3D quantification methods, however, Rudow et al (23) reported an age-associated increase of neuronal size on the substantia nigra using the nucleator method, whereas Cabello et al (24) demonstrated no decrease by using the rotator method; thus, there is similar disagreement as that generated using 2D studies. Because each of these groups was careful to ensure that the method of volume estimation used was unbiased, these conflicting results may be related to methodologic differences and their limitations.

Instead of using these indirect estimation methods, our direct method quantified the actual volume of nuclei reconstructed from serially obtained optical sections spanning the entire structure of oligodendrocytes, including the nucleus and GCIs when they were. To our knowledge, this is the first successful attempt to quantify directly the volume of pathologic structures in the human brain on a 3D basis. Because this strategy deals with the 3D reality and its direct measurement, it is completely free from bias that may derive from both sampling and estimation. The normal size distribution of the measured nuclear volumes in each case confirmed the reliability of our method of sampling and volumetry.

Using this method, we demonstrated that the nuclear volume of oligodendroglia in MSA is significantly smaller as a whole than in the control group, and that, although the nuclear volume of GCI^+ oligodendrocytes was equivalent to that of the control group, the GCI^- oligodendrocytes are responsible for this volume reduction, that is, nuclear shrinkage seems to be accelerated in the absence of GCIs (Table 2).

Because the absence of significant differences among groups for age and sex might have been related to a limited number of cases with wide ranges of age at death (Table 1), statistical analyses were performed after omitting the youngest patient (Control 1; 47 years at death) to determine whether the exaggerated difference in age might give alternative results. Omission of Control 1 (203.82 ± 64.37 μm^3; $n = 21$) did not result in a significant change in nuclear volume (new control group: 186.90 ± 54.97 μm^3; $n = 287$ vs entire control group, 188.05 ± 55.71 μm^3; $n = 308$, $p > 0.05$ or vs Control 1, $p > 0.05$ by Student t-test). This replicated the significant differences seen before the omission, that is, the GCI^+ group and the new control group are larger than the GCI^- group ($p < 0.001$ by 1-way ANOVA), and the GCI^+ and the new control group are not significantly different ($p > 0.05$ by 1-way ANOVA). Although this study was not designed to identify age-related changes in the nuclear volume of oligodendrocytes, the size distributions of each group (GCI^+, GCI^-, and control) were compatible with the normal size distribution, suggesting that our sampling and volumetric procedures were appropriate to represent a single cell group corresponding to each category. Thus, it is clear that reduction of nuclear volume is evident exclusively in the GCI^- group even if there were potentially confounding age-related changes.

It has been generally considered that the size/volume of the nuclei, nucleoli, and cell body of neurons undergo

TABLE 3. Three-Dimensional Volume Estimates and Their Changes in Relation to Aging and Degeneration

		Overall Change, %	Reference
Aging	SN neuron, TH^+*	+39 in SN neuron, +23 in TH^+	23
	SN m^+ neuron†	No decrease	24
	NC neuron†	Decrease	25
PD	SN neuron*	Reduction	23
AD	ACG, PCG, CA1, PVC nucleolus, nuclei, neuron*	Hypertrophy in CA1/ACG of asymptomatic AD	26
ALS	MC nuclei, neuron†	No difference	27
TLE	TC neuron*	+28 in GM,+55 in WM	28
Alcoholics	Purkinje cell/nuclei, neuron†	−24 in cell body, −16 in nuclei	29

*The nucleator method and its modifications.
†The rotator method and its modifications.
ACG, anterior cingulate gyrus; AD, Alzheimer disease; ALS, amyotrophic lateral sclerosis; CA1, Cornu ammonis 1; GM, gray matter; m^+, melanin-positive; MC, motor cortex; NC, neocortex; PCG, posterior cingulate gyrus; PD, Parkinson disease; PVC, primary visual cortex; SN, substantia nigra; TC, temporal cortex; TH^+, tyrosine hydroxylase–positive neuron; TLE, temporal lobe epilepsy; WM, white matter.

shrinkage in aging and neurodegenerative processes. As expected, therefore, we demonstrated that the nuclear volumes of oligodendroglia in MSA cases as a whole are significantly reduced. Table 3 shows the summary of indirect 3D estimation of the volume of the nucleoli/nuclei/cell and their relation to aging and diseases; neurodegenerative processes are not necessarily related to volume reduction of neurons (26–28). Because these data were obtained without distinguishing the presence or absence of pathologic inclusions, however, how the disease-related changes identified are linked to pathologic inclusions is unclear. Indeed, several 2D morphometric studies have focused on the size of individual cells to identify cellular changes and their relationships to pathologic inclusions (Table 4). For example, transected nuclear areas of pontine neurons harboring nuclear inclusions are uniformly larger than those not harboring nuclear inclusions (32–34). Two-dimensional observations of a thin histologic plane may, however, not identify inclusions within the cell that are not present in the histologic plane. Our 3D reconstruction analysis spans the entire target structure, including pathologic inclusions, and therefore definitively determines whether or not pathologic inclusions are present. Although the relationships between disease-related changes and inclusion-related changes remain to be clarified, it is now possible to quantify 3D changes of each cell without bias after definitively determining the presence or absence of pathologic inclusions.

It is not surprising that the pathologic inclusions in MSA are related to a larger cell/nuclear size or a lesser extent of degeneration. There are similar examples in cell culture models (36, 37), transgenic animals (38, 39), and a variety of human conditions (30–35). It is not clear whether oligodendrocytes with and without GCI undergo completely different degenerative processes or whether they represent different aspects of a shared process. Because the distribution of the nuclear volume of MSA oligodendrocytes as a whole was neither unimodal (single peak) nor bimodal (double peaks; Fig. 2), it is likely that the GCI^+ and GCI^- groups undergo some common mechanism of the degeneration. The selective decrease in nuclear volume restricted to the GCI^- group cannot be explained if the nuclear shrinkage is accelerated in the presence of GCIs. Preserved nuclear volume of GCI^+ oligodendrocytes does not necessarily imply that they are free from the degenerative process.

Some studies have attempted to simulate the oligodendroglial pathology of MSA. For example, overexpression of human α-synuclein leads to the cytotoxicity in cultured oligodendrocytic progenitor cells (40), and transgenic mice that overexpress human wild-type α-synuclein show progressive locomotor dysfunction; histologic analyses showed the accumulation of detergent-insoluble α-synuclein similar to GCIs (41, 42) and system-oriented degeneration but with some differences from MSA (43, 44). Numerous studies of MSA patient brains have attempted to find possible correlations between GCIs and degeneration. In MSA, GCIs show a "system-oriented distribution in the suprasegmental motor systems (i.e. primary motor and higher motor areas of the cerebral cortex, pyramidal, extrapyramidal, and corticocerebellar systems) in the supraspinal autonomic systems and in their targets" (4), and changes in neurons follow a similar distribution pattern (2, 4, 6). Nevertheless, the density of GCIs and the severity of neuronal loss and their possible correlations claimed by previous studies are highly conflicting (2, 4, 6, 7, 45). Apoptosis-related proteins, including Bax (46) and activated caspase 3 (47), are reportedly present mainly in oligodendrocytes, often showing α-synuclein–positive inclusions (47). Interestingly, the cytoplasmic expression of Bcl-2, a putative anti-apoptotic protein, has been reported in oligodendrocytes with α-synuclein coexpression in approximately 25% of GCI^+ cells (46). Although the major question of whether GCIs are cytotoxic or cytoprotective remains to be answered, apoptosis with the morphologic feature of nuclear shrinkage (48) is considered to account for at least some of the oligodendroglial death in MSA (46, 47). In Parkinson disease and dementia with Lewy bodies (other degenerative processes with α-synuclein deposits [49, 50]), it is hypothesized that the aggregation of α-synuclein prevents or delays neuronal degeneration possibly by sequestering toxic protein species (51, 52). It remains to be determined whether a similar scenario may also explain the role of aggregation of α-synuclein as GCIs in MSA. The relative preservation of nuclear volume with GCI and accelerated shrinkage in the absence of GCIs in human brain are compatible with this possibility.

It is now possible to analyze the pathologic expression of specific molecules in relation to nuclear size. Molecular mechanisms bridging cellular/nuclear atrophy and GCI formation or other pathologic deposits are now candidate subjects for further study in a quantitative fashion rather than a "black and white" dualism such as neuronal death versus survival. The novel strategy for human brain studies used herein provides a pivotal viewpoint regarding the pathologic significance of GCIs and will be applicable to degenerative processes other than MSA.

TABLE 4. Two-Dimensional Area Quantification Studies and Their Dependence on Index Lesions

	Target ± Index Lesion/Area	Change of Area Dependent on the Index Lesion, %	Reference
PD	SN neuron ± LBs/nucleolus, neuron	No difference	30
AD	Hippocampal neuron ± NFTs/nucleolus, neuron	No difference	31
MJD	Pontine neuron ± NAs/nucleus	−21% with NAs, −41% without NAs	32
NIID	Pontine neuron ± NIIs/nucleus	+22% with NIIs, −14% without NIIs	33
SCA1	Pontine neuron ± NIs/nucleus	No difference with NIs, −12% without NIs	34
DRPLA	Cerebellar granule cell ± NIIs/nucleus	Larger with NIIs	35

±, with/without; AD, Alzheimer disease; DRPLA, dentatorubral-pallidoluysian atrophy; LBs, Lewy bodies; MJD, Machado-Joseph disease; NA, nuclear aggregate; NFTs, neurofibrillary tangles; NI, nuclear inclusion; NII, neuronal intranuclear inclusion; NIID, neuronal intranuclear inclusion disease; PD, Parkinson disease; SCA1, spinocerebellar ataxia 1; SN, substantia nigra.

ACKNOWLEDGMENTS

The authors thank Prof Hidekazu Tomimoto, MD, PhD, Department of Neurology, Mie University, Japan, and Hideaki Hayashi, MD, PhD, the former director of Tokyo Metropolitan Neurological Hospital, Japan, for their valuable help.

REFERENCES

1. Graham JG, Oppenheimer DR. Orthostatic hypotension and nicotine sensitivity in a case of multiple system atrophy. J Neurol Neurosurg Psychiatry 1969;32:28–34
2. Papp MI, Kahn JE, Lantos PL. Glial cytoplasmic inclusions in the CNS of patients with multiple system atrophy (striatonigral degeneration, olivopontocerebellar atrophy and Shy-Drager syndrome). J Neurol Sci 1989;94:79–100
3. Nakazato Y, Yamazaki H, Hirato J, et al. Oligodendroglial microtubular tangles in olivopontocerebellar atrophy. J Neuropathol Exp Neurol 1990; 49:521–30
4. Papp MI, Lantos PL. The distribution of oligodendroglial inclusions in multiple system atrophy and its relevance to clinical symptomatology. Brain 1994;117:235–43
5. Armstrong RA, Cairns NJ, Lantos PL. A quantitative study of the pathological changes in ten patients with multiple system atrophy (MSA). J Neural Transm 2004;111:485–95
6. Ozawa T, Paviour D, Quinn NP, et al. The spectrum of pathological involvement of the striatonigral and olivopontocerebellar systems in multiple system atrophy: Clinicopathological correlations. Brain 2004; 127:2657–71
7. Inoue M, Yagishita S, Ryo M, et al. The distribution and dynamic density of oligodendroglial cytoplasmic inclusions (GCIs) in multiple system atrophy: A correlation between the density of GCIs and the degree of involvement of striatonigral and olivopontocerebellar systems. Acta Neuropathol 1997;93:585–91
8. Mochizuki A, Mizusawa H, Ohkoshi N, et al. Argentophilic intracytoplasmic inclusions in multiple system atrophy. J Neurol 1992;239: 311–16
9. Abe H, Yagishita S, Amano N, et al. Argyrophilic glial intracytoplasmic inclusions in multiple system atrophy: Immunocytochemical and ultrastructural study. Acta Neuropathol 1992;84:273–77
10. Jensen EBV, Gundersen HJG. The rotator. J Microsc 1993;170:35–44
11. Gundersen HJG. The nucleator. J Microsc 1988;151:3–21
12. Gundersen HJG, Jensen EBV. The efficiency of systematic sampling in stereology and its prediction. J Microsc 1987;147:229–63
13. Rudin W. The Riemann-Stieltjes integral. In: Rudin W ed. *Principles of Mathematical Analysis*. 2nd ed. New York, NY: McGraw-Hill, 1964: 104–29
14. McNeal GR, Maynard WH, Branch RA, et al. Liver volume measurements and three-dimensional display from MR images. Radiology 1988; 169:851–54
15. Bakker J, Olree M, Kaatee R, et al. Renal volume measurements: Accuracy and repeatability of US compared with that of MR imaging. Radiology 1999;211:623–28
16. Kubínová L, Janácek J, Guilak F, et al. Comparison of several digital and stereological methods for estimating surface area and volume of cells studied by confocal microscopy. Cytometry 1999;36:85–95
17. Kanazawa T, Uchihara T, Takahashi A, et al. Three-layered structure shared between Lewy bodies and Lewy neurites-three-dimensional reconstruction of triple-labeled sections. Brain Pathol 2008;18:415–22
18. Suzuki M, Raisman G. The glial framework of central white matter tracts: Segmented rows of contiguous interfascicular oligodendrocytes and solitary astrocytes give rise to a continuous meshwork of transverse and longitudinal processes in the adult rat fimbria. Glia 1992;6: 222–35
19. Ma SY, Röytt M, Collan Y, et al. Unbiased morphometrical measurements show loss of pigmented nigral neurones with ageing. Neuropathol Appl Neurobiol 1999;25:394–99
20. Cruz-Sánchez FF, Cardozo A, Tolosa E. Neuronal changes in the substantia nigra with aging: A Golgi study. J Neuropathol Exp Neurol 1995;54:74–81
21. Neal JW, Pearson RC, Cole G, et al. Neuronal hypertrophy in the pars reticulata of the substantia nigra in Parkinson's disease. Neuropathol Appl Neurobiol 1991;17:203–6
22. Ma SY, Rinne JO, Collan Y, et al. A quantitative morphometrical study of neuron degeneration in the substantia nigra in Parkinson's disease. J Neurol Sci 1996;140:40–45
23. Rudow G, O'Brien R, Savonenko AV, et al. Morphometry of the human substantia nigra in ageing and Parkinson's disease. Acta Neuropathol 2008;115:461–70
24. Cabello CR, Thune JJ, Pakkenberg H, et al. Ageing of substantia nigra in humans: Cell loss may be compensated by hypertrophy. Neuropathol Appl Neurobiol 2002;28:283–91
25. Stark AK, Toft MH, Pakkenberg H, et al. The effect of age and gender on the volume and size distribution of neocortical neurons. Neuroscience 2007;150:121–30
26. Iacono D, O'Brien R, Resnick SM, et al. Neuronal hypertrophy in asymptomatic Alzheimer disease. J Neuropathol Exp Neurol 2008;67: 578–89
27. Toft MH, Gredal O, Pakkenberg B. The size distribution of neurons in the motor cortex in amyotrophic lateral sclerosis. J Anat 2005;207: 399–407
28. Bothwell S, Meredith GE, Phillips J, et al. Neuronal hypertrophy in the neocortex of patients with temporal lobe epilepsy. J Neurosci 2001;21: 4789–800
29. Andersen BB. Reduction of Purkinje cell volume in cerebellum of alcoholics. Brain Res 2004;1007:10–18
30. Gertz HJ, Siegers A, Kuchinke J. Stability of cell size and nucleolar size in Lewy body containing neurons of substantia nigra in Parkinson's disease. Brain Res 1994;637:339–41
31. Gertz HJ, Schoknecht G, Krüger H, et al. Stability of cell size and nucleolar size in tangle-bearing neurons of the hippocampus in Alzheimer's disease. Brain Res 1989;487:373–75
32. Uchihara T, Iwabuchi K, Funata N, et al. Attenuated nuclear shrinkage in neurons with nuclear aggregates-a morphometric study on pontine neurons of Machado-Joseph disease brains. Exp Neurol 2002;178: 124–28
33. Uchihara T, Tanaka J, Funata N, et al. Influences of intranuclear inclusion on nuclear size—Morphometric study on pontine neurons of neuronal intranuclear inclusion disease cases. Acta Neuropathol 2003; 105:103–8
34. Nagaoka U, Uchihara T, Iwabuchi K, et al. Attenuated nuclear shrinkage in neurones with nuclear inclusions of SCA1 brains. J Neurol Neurosurg Psychiatry 2003;74:597–601
35. Takahashi H, Egawa S, Piao YS, et al. Neuronal nuclear alterations in dentatorubral-pallidoluysian atrophy: Ultrastructural and morphometric studies of the cerebellar granule cells. Brain Res 2001;919:12–19
36. Saudou F, Finkbeiner S, Devys D, et al. Huntingtin acts in the nucleus to induce apoptosis but death does not correlate with the formation of intranuclear inclusions. Cell 1998;95:55–66
37. Arrasate M, Mitra S, Schweitzer ES, et al. Inclusion body formation reduces levels of mutant huntingtin and the risk of neuronal death. Nature 2004;431:805–10
38. Yamamoto A, Lucas JJ, Hen R. Reversal of neuropathology and motor dysfunction in a conditional model of Huntington's disease. Cell 2000; 101:57–66
39. Klement IA, Skinner PJ, Kaytor MD, et al. Ataxin-1 nuclear localization and aggregation: role in polyglutamine-induced disease in SCA1 transgenic mice. Cell 1998;95:41–53
40. Tsuboi K, Grzesiak JJ, Bouvet M, et al. Alpha-synuclein overexpression in oligodendrocytic cells results in impaired adhesion to fibronectin and cell death. Mol Cell Neurosci 2005;29:259–68
41. Yazawa I, Giasson BI, Sasaki R, et al. Mouse model of multiple system atrophy α-synuclein expression in oligodendrocytes causes glial and neuronal degeneration. Neuron 2005;45:847–59
42. Kahle PJ, Neumann M, Ozmen L, et al. Hyperphosphorylation and insolubility of α-synuclein in transgenic mouse oligodendrocytes. EMBO Rep 2002;3:583–88
43. Shults CW, Rockenstein E, Crews L, et al. Neurological and neurodegenerative alterations in a transgenic mouse model expressing human α-synuclein under oligodendrocyte promoter: Implications for multiple system atrophy. J Neurosci 2005;25:10689–99
44. Stefanova N, Reindl M, Neumann M, et al. Oxidative stress in transgenic mice with oligodendroglial α-synuclein overexpression replicates the